Dartmouth College
Dartmouth Digital Commons

Dartmouth Scholarship | Faculty Work

9-2011

Type II Toxoplasma Gondii KU80 Knockout Strains Enable Functional Analysis of Genes Required for Cyst Development and Latent Infection

Barbara A. Fox
Dartmouth College

Alejandra Falla
Dartmouth College

Leah M. Rommereim
Dartmouth College

Tadakimi Tomita
Dartmouth College

Follow this and additional works at: https://digitalcommons.dartmouth.edu/facoa

 Part of the Genetics Commons, and the Pathogenic Microbiology Commons

Dartmouth Digital Commons Citation

Fox, Barbara A.; Falla, Alejandra; Rommereim, Leah M.; and Tomita, Tadakimi, "Type II Toxoplasma Gondii KU80 Knockout Strains Enable Functional Analysis of Genes Required for Cyst Development and Latent Infection" (2011). *Dartmouth Scholarship*. 821.
https://digitalcommons.dartmouth.edu/facoa/821

This Article is brought to you for free and open access by the Faculty Work at Dartmouth Digital Commons. It has been accepted for inclusion in Dartmouth Scholarship by an authorized administrator of Dartmouth Digital Commons. For more information, please contact dartmouthdigitalcommons@groups.dartmouth.edu.

EUKARYOTIC CELL, Sept. 2011, p. 1193–1206 Vol. 10, No. 9
1535-9778/11/$12.00 doi:10.1128/EC.00297-10
Copyright © 2011, American Society for Microbiology. All Rights Reserved.

Type II *Toxoplasma gondii KU80* Knockout Strains Enable Functional Analysis of Genes Required for Cyst Development and Latent Infection[▽]†

Barbara A. Fox,[1] Alejandra Falla,[1] Leah M. Rommereim,[1] Tadakimi Tomita,[2] Jason P. Gigley,[1]‡ Corinne Mercier,[3] Marie-France Cesbron-Delauw,[3] Louis M. Weiss,[2] and David J. Bzik[1]*

Department of Microbiology and Immunology, Dartmouth Medical School, 1 Medical Center Drive, Lebanon, New Hampshire 03756[1]; Departments of Medicine and Pathology, Albert Einstein College of Medicine, 1300 Morris Park Avenue, Bronx, New York 10461[2]; and Laboratoire Adaptation et Pathogénie des Microorganismes, UMR 5163 CNRS, Université Grenoble 1, Institute Jean Roget, 38700 La Tronche, France[3]

Received 29 November 2010/Accepted 17 April 2011

Type II *Toxoplasma gondii KU80* knockouts (Δ*ku80*) deficient in nonhomologous end joining were developed to delete the dominant pathway mediating random integration of targeting episomes. Gene targeting frequency in the type II Δ*ku80* Δ*hxgprt* strain measured at the orotate (*OPRT*) and the uracil (*UPRT*) phosphoribosyltransferase loci was highly efficient. To assess the potential of the type II Δ*ku80* Δ*hxgprt* strain to examine gene function affecting cyst biology and latent stages of infection, we targeted the deletion of four parasite antigen genes (*GRA4*, *GRA6*, *ROP7*, and *tgd057*) that encode characterized CD8$^+$ T cell epitopes that elicit corresponding antigen-specific CD8$^+$ T cell populations associated with control of infection. Cyst development in these type II mutant strains was not found to be strictly dependent on antigen-specific CD8$^+$ T cell host responses. In contrast, a significant biological role was revealed for the dense granule proteins GRA4 and GRA6 in cyst development since brain tissue cyst burdens were drastically reduced specifically in mutant strains with *GRA4* and/or *GRA6* deleted. Complementation of the Δ*gra4* and Δ*gra6* mutant strains using a functional allele of the deleted *GRA* coding region placed under the control of the endogenous *UPRT* locus was found to significantly restore brain cyst burdens. These results reveal that GRA proteins play a functional role in establishing cyst burdens and latent infection. Collectively, our results suggest that a type II Δ*ku80* Δ*hxgprt* genetic background enables a higher-throughput functional analysis of the parasite genome to reveal fundamental aspects of parasite biology controlling virulence, pathogenesis, and transmission.

Toxoplasma gondii is an extremely widespread obligate intracellular protozoan pathogen of virtually all warm-blooded animals (19). Infection is initiated following oral ingestion of transmissible parasite stages included within cysts contained in infected meat or within oocysts released in the environment by cat feces. Primary *T. gondii* infection rarely causes significant disease in the nonimmunocompromised individual, unless infection is transmitted *in utero* (50). Latent *T. gondii* infection is characterized by the presence of tissue cysts containing nonreplicating bradyzoites. The cysts persist primarily in muscles, the eyes, and the brain (19). For unknown reasons, latent tissue cysts occasionally rupture, and this cyst reactivation can lead to recrudescent disease. By example, infection *in utero* is associated with the highest risk of later development of ocular toxoplasmosis (66), a significant recurrent retinal infection (36). Immunosuppression markedly increases the likelihood of cyst rupture, conversion of latent bradyzoites to rapidly dividing tachyzoites, and the development of reactivated disease (51). Immune control of latent infection fails in AIDS and other severe immunodeficiencies, resulting in a recrudescent acute infection and causing a potentially lethal toxoplasmic encephalitis (12).

T. gondii has rapidly developed as an outstanding model organism for obligate intracellular eukaryotic pathogens (40, 53). Within the single genus and species *T. gondii*, three major strain types were defined by their virulence phenotype in mice (58). Currently, type I strains of *T. gondii* are excellent *in vitro* models, but this acutely virulent strain type does not readily develop tissue cysts or latent infection in laboratory mice. In contrast, type II strains of *T. gondii* easily establish latent infections in mice that are characterized by the presence of tissue cysts, the key obligate developmental and latent stage required for the remarkably high transmission potential of this parasite (52). Oral transmission appears to have driven the recent clonal expansion of strains that predominate in North America and Europe (62). Type II strains represent the most prevalent strain type chronically infecting North American and European populations (33). After oral ingestion of a tissue cyst in a naive host, the encysted bradyzoite reactivates and converts back to the rapidly dividing tachyzoite form that causes disseminated acute infection, followed later by cyst development and the establishment of a latent infection in the host (19).

* Corresponding author. Mailing address: Department of Microbiology and Immunology, Dartmouth Medical School, 1 Medical Center Dr., Lebanon, NH 03756. Phone: (603) 650-7951. Fax: (603) 650-6223. E-mail: david.j.bzik@dartmouth.edu.

† Supplemental material for this article may be found at http://ec.asm.org/.

‡ Present address: Department of Microbiology, Immunology, and Tropical Medicine, George Washington University Medical Center, 2300 I St. NW, Washington, DC 20037.

▽ Published ahead of print on 29 April 2011.

While induction of tachyzoite to bradyzoite conversion *in vitro* can be triggered by various stress responses (temperature, high pH, chemical stress, nutrient stress, and cytokines) (67), little is currently known regarding fundamental parasite biology underlying acute and latent phases of infection *in vivo*.

Host-parasite interaction in acute and latent phases of type II *T. gondii* infection is dynamic. During acute infection *T. gondii* selectively invades host cell types primarily of the dendritic, macrophage, and neutrophil lineages (4, 11, 31). By invading host cell types that are critical to mounting effective innate responses to infection, the parasite actively seeks to manipulate the host through several mechanisms (14). Despite or because of this strategy, the host rapidly mounts highly effective $CD8^+$ T cell responses associated with strong interferon gamma (IFN-γ) responses (26, 58). These innate and adaptive immune responses are required to achieve control of acute infection and may also trigger tachyzoite to bradyzoite conversion and development of the latent transmissible tissue cyst (29, 63, 67).

Several landmark studies have recently identified four parasite antigen genes (*GRA4*, *GRA6*, *ROP7*, and *tgd057*) that possess $CD8^+$ T cell epitopes that elicit corresponding antigen-specific $CD8^+$ T cells associated with the immune control of *T. gondii* infection (5, 27, 42, 68). The ROP7 protein of unknown function belongs to a family of rhoptry proteins localized to the parasite rhoptry organelles. These Apicomplexa-specific secretory organelles discharge their contents into the host cytosol during invasion of the host cell (7). The parasite dense granule (GRA) proteins GRA4 and GRA6 are members of the *Toxoplasma* prominent dense granule protein family (46, 49). Dense granule proteins are highly expressed proteins. The dense granule secretory organelles discharge their contents into the parasitophorous vacuole (PV) space following host cell invasion and the initial formation of the parasitophorous vacuole membrane (PVM) (9). A newly proposed member of the dense granule protein family called GRA15 localized to the dense granules, the PV space, the space outside of the PVM, and was also associated with evacuoles, suggesting that GRA15 is also a rhoptry-like protein in potentially being secreted during invasion of the host cell (54). GRA15 plays a significant role in host cell NF-κB nuclear translocation and NF-κB-mediated transcription and regulates the induction of IL-12 secretion in infected mouse macrophages (54). Various potential biological roles for GRA proteins have been previously proposed and significant studies have been performed on GRA protein secretion, traffic, and interaction biology (10, 49). At the tachyzoite stage, most of the GRA proteins associate with the PV membranes, meaning either the PVM and its digitations or the intravacuolar network of membranous tubules (49). At the bradyzoite stage, most of the GRA proteins were localized at the cyst wall or in the cyst matrix (64).

Type I mutants deleted in GRA2 or GRA6 showed a phenotype of reduced acute virulence during infection in mice (48; C. Mercier, unpublished data). However, to date, the only GRA proteins successfully disrupted in the type II background are GRA3 (13) and GRA15 (54). Disruption of type II *GRA3* resulted in a phenotype of reduced acute virulence (13). Disruption of type II *GRA15* increased parasite burdens in infected mice without influencing virulence (54). These previous studies did not address a functional role for GRA proteins in cyst development during infection. While GRA proteins appear to be central to the host-parasite relationship, it is currently unknown whether GRA proteins are required to establish latent infection.

Tachyzoite-to-bradyzoite conversion, cyst development, and latent infection are critical to parasite survival and transmission. Nine distinct targeted gene deletions (1, 6, 13, 32, 38, 54, 55, 57, 65, 69) have been successfully developed in type II strains since genetic transformation of *T. gondii* was reported nearly 20 years ago (18, 39, 61). In contrast, recently reported type I *KU80* knockout strains that exhibit highly efficient gene replacement frequencies has significantly accelerated the development of targeted gene deletions (2, 3, 15, 20, 23, 26, 34, 37, 44). Increased efficiency of double-crossover homologous recombination at targeted loci in *KU80* knockouts is due to the functional loss of the nonhomologous end-joining DNA repair pathway that mediates a major mechanism underlying frequent random insertion of linear episomes in *T. gondii* (26). We report here the development of *KU80* knockouts (Δ*ku80*) in type II *T. gondii*. Eight genetic loci were targeted for the development of mutant strains with targeted single-gene deletions or multiple-gene deletions to functionally examine candidate genes required for cyst development and latent infection. In particular, we examined the hypothesis that a host response to parasite antigen genes that elicit antigen-specific $CD8^+$ T cell responses during host infection may be essential to cyst development. Our results support a critical role for dense granule proteins GRA4 and GRA6 in fundamental biology at the host-parasite interface that is essential for cyst development and transmission of *T. gondii*.

MATERIALS AND METHODS

Primers. All oligonucleotide primers used in the development of plasmids for targeting gene deletions are listed in Table S1 in the supplemental material. All oligonucleotide primers used in validation of mutants with gene deletions are listed in Table S2 in the supplemental material.

Plasmid constructs. All plasmids were developed using the yeast shuttle vector pRS416 and yeast recombination cloning which fused three distinct genetic elements (an ~1-kb 5′ target flank, an ~2-kb hypoxanthine-xanthine-guanine phosphoribosyltransferase [*HXGPRT*] selectable marker cassette, and an ~1-kb 3′ target flank, all 5′ to 3′ and in this order) with pRS416 using 31- to 33-bp homologous crossovers at recombination junctions (23). DNA elements for yeast recombination were amplified from type II Prugniaud (Pru) genomic DNA or type I RH genomic DNA as indicated. Targeting plasmids constructed in pRS416 were verified by using restriction enzyme digests, and target DNA flanks were sequenced to verify DNA sequence homology.

Plasmid pΔTPR1 was constructed to delete nucleotides 2741952 to 2737843 in the Pru *KU80* locus, defined as TGME49_112510 on chrXI of the ToxoDB database version 6.0 (www.toxodb.org). This deletion strategy deletes 1,228 bp of the *KU80* 5′ upstream putative gene regulatory region and the first three exons of the predicted four protein coding exons of the *KU80* gene. The *HXGPRT* minigene cassette was fused between a 2,997-bp 5′ genomic targeting flank and a 3,304-bp 3′ genomic targeting flank amplified from Pru genomic DNA.

Plasmid pΔTPFC1 was constructed by NotI and PmeI digestion of pΔTPR1 at the 3′ end of the 3′ targeting flank, followed by ligation with the cytosine deaminase (CD) selectable marker contained on a NotI/PmeI restriction fragment isolated from plasmid pMCD4.4 (26).

Plasmid pΔTPRC2 was constructed by digesting pΔTPR1 with KspI, followed by self-ligation to delete the *HXGPRT* minicassette fragment from pΔTPR1.

Plasmid pΔUPRP was constructed to delete nucleotides 2709350 to 2713372 of the uracil phosphoribosyltransferase (*UPRT*) chromosomal locus on chrXI annotated as TGME49_112480. The *HXGPRT* minigene cassette was fused between a 1,131-bp 5′ *UPRT* genomic targeting flank and a 1,119-bp 3′ *UPRT* genomic targeting flank amplified from Pru genomic DNA.

Plasmid pΔUPP was constructed to delete nucleotides 1491873 to 1488688 of

TABLE 1. *T. gondii* strains used and developed in this study[a]

Strain	Parent strain (source or reference)	Genotype
PruΔ*ku80*::*HXGPRT*	PruΔ*hxgprt* (BSG-4) (60)	Δ*ku80*
PruΔ*ku80*Δ*hxgprt*	PruΔ*ku80*::*HXGPRT*	Δ*ku80* Δ*hxgprt*
PruΔ*ku80*Δ*uprt*::*HXGPRT*	PruΔ*ku80*Δ*hxgprt*	Δ*ku80* Δ*uprt*::*HXGPRT*
RHΔ*ku80*Δ*oprt*::*HXGPRT*	RHΔ*ku80*Δ*hxgprt* (26)	Δ*ku80* Δ*oprt*::*HXGPRT*
PruΔ*ku80*Δ*oprt*::*HXGPRT*	PruΔ*ku80*Δ*hxgprt*	Δ*ku80* Δ*oprt*::*HXGPRT*
PruΔ*ku80*Δ*oprt*Δ*hxgprt*	PruΔ*ku80*Δ*oprt*::*HXGPRT*	Δ*ku80* Δ*oprt* Δ*hxgprt*
PruΔ*ku80*Δ*up*::*HXGPRT*	PruΔ*ku80*Δ*hxgprt*	Δ*ku80* Δ*up*::*HXGPRT*
PruΔ*ku80*Δ*gra4*::*HXGPRT*	PruΔ*ku80*Δ*hxgprt*	Δ*ku80* Δ*gra4*::*HXGPRT*
PruΔ*ku80*Δ*gra4*Δ*hxgprt*	PruΔ*ku80*Δ*gra4*::*HXGPRT*	Δ*ku80* Δ*gra4* Δ*hxgprt*
PruΔ*ku80*Δ*gra6*::*HXGPRT*	PruΔ*ku80*Δ*hxgprt*	Δ*ku80* Δ*gra6*::*HXGPRT*
PruΔ*ku80*Δ*gra6*Δ*hxgprt*	PruΔ*ku80*Δ*gra6*::*HXGPRT*	Δ*ku80* Δ*gra6* Δ*hxgprt*
PruΔ*ku80*Δ*tgd057*::*HXGPRT*	PruΔ*ku80*Δ*hxgprt*	Δ*ku80* Δ*tgd057*::*HXGPRT*
PruΔ*ku80*Δ*rop4*/*7*::*HXGPRT*	PruΔ*ku80*Δ*hxgprt*	Δ*ku80* Δ*rop4*/*7*::*HXGPRT*
PruΔ*ku80*Δ*gra4*Δ*tgd057*::*HXGPRT*	PruΔ*ku80*Δ*gra4*Δ*hxgprt*	Δ*ku80* Δ*gra4* Δ*tgd057*::*HXGPRT*
PruΔ*ku80*Δ*gra6*Δ*tgd057*::*HXGPRT*	PruΔ*ku80*Δ*gra6*Δ*hxgprt*	Δ*ku80* Δ*gra6* Δ*tgd057*::*HXGPRT*
PruΔ*ku80*Δ*gra6*Δ*gra4*::*HXGPRT*	PruΔ*ku80*Δ*gra6*Δ*hxgprt*	Δ*ku80* Δ*gra6* Δ*gra4*::*HXGPRT*
PruΔ*ku80*Δ*gra6*Δ*gra4*Δ*hxgprt*	PruΔ*ku80*Δ*gra6*Δ*gra4*::*HXGPRT*	Δ*ku80* Δ*gra6* Δ*gra4* Δ*hxgprt*
PruΔ*ku80*Δ*gra4*Δ*uprt*::*gra4*$^{\text{coding region + 3'UTR}}$*HXGPRT*	PruΔ*ku80*Δ*gra4*Δ*hxgprt*	Δ*ku80* Δ*gra4* Δ*uprt*::*gra4*$^{\text{coding region + 3'UTR}}$ *HXGPRT*
PruΔ*ku80*Δ*gra6*Δ*uprt*::*gra6*$^{\text{coding region + 3'UTR}}$*HXGPRT*	PruΔ*ku80*Δ*gra6*Δ*hxgprt*	Δ*ku80* Δ*gra6* Δ*uprt*::*gra6*$^{\text{coding region + 3'UTR}}$ *HXGPRT*

[a] All strains used and developed in this study are transgenic for *LDH2-GFP* and the chloramphenicol drug resistance marker (*CAT*) randomly integrated into the parental Pru strain at undefined genetic loci (60).

the uridine phosphorylase (*UP*) chromosomal locus (23) on chrXI annotated as TGME49_110640. The *HXGPRT* minigene cassette was fused between a 1,141-bp 5′ *UP* genomic targeting flank and a 955-bp 3′ *UP* genomic targeting flank amplified from Pru genomic DNA.

Plasmid pΔOPT was constructed to delete nucleotides 2733578 to 2735556 of the orotate phosphoribosyltransferase (*OPRT*) locus defined as TGGT1_010360 on chrVIIb. The *HXGPRT* minigene cassette was fused between a 1,050-bp 5′ *OPRT* genomic targeting flank and a 1,118-bp 3′ *OPRT* genomic targeting flank amplified from RH genomic DNA.

Plasmid pΔOPP was constructed to delete nucleotides 2719166 to 2721148 of the *OPRT* locus defined as TGME49_059660 on chrVIIb. The *HXGPRT* minigene cassette was fused between a 1,050-bp 5′ *OPRT* genomic targeting flank and a 1,118-bp 3′ *OPRT* genomic targeting flank amplified from Pru genomic DNA.

Plasmid pΔOPPC was constructed by digesting pΔOPP with SacII, followed by self-ligation to delete the *HXGPRT* minicassette.

Plasmid pΔGRA4P was constructed to delete nucleotides 1581347 to 1570147 of the *GRA4* locus on chrXI annotated as TGME49_110780. The *HXGPRT* minigene cassette was fused between a 1,124-bp 5′ *GRA4* genomic targeting flank and a 989-bp 3′ *GRA4* genomic targeting flank amplified from Pru genomic DNA.

Plasmid pΔGRA4PC was constructed by digesting pΔGRA4 with SpeI, followed by self-ligation to delete the *HXGPRT* minicassette.

Plasmid pΔGRA6P was constructed to delete nucleotides 7216123 to 7215219 of the *GRA6* locus on chrX annotated as TGME49_075440. The *HXGPRT* minigene cassette was fused between a 1,048-bp 5′ *GRA6* genomic targeting flank and a 955-bp 3′ *GRA6* genomic targeting flank amplified from Pru genomic DNA.

Plasmid pΔGRA6PC was constructed by digesting pΔGRA6 with SpeI, followed by self-ligation to delete the *HXGPRT* minicassette.

Plasmid pΔROP4/7P was constructed to delete nucleotides 1414364 to 1404628 of the *ROP4*/*7* locus on chr1a annotated as TGME49_095110. This gene locus is incomplete in the genome database. Analysis of the Toxodb database identified common flanking and unique DNA surrounding the *ROP4*/*7* locus and suggested the gene structure for the *ROP4*/*7* locus consists of a 5′ *ROP4* gene, followed by a complete *ROP7A* allele and *ROP7B* allele (with identical coding DNA but minor polymorphisms in their UTRs) and a 3′ truncated and incomplete *ROP7C* allele (L. M. Rommereim and D. J. Bzik, unpublished data). Consequently, we targeted the deletion of the entire locus (~14,297 bp) and all *ROP4* and *ROP7* alleles by using target DNA flanks derived from unique DNA sequences that reside just 5′ or just 3′ of the *ROP4*/*7* locus. The *HXGPRT* minigene cassette was fused between a 1,179-bp 5′ *ROP4*/*7* genomic targeting flank and a 989-bp 3′ *ROP4*/*7* genomic targeting flank amplified from Pru genomic DNA.

Plasmid pΔTGD057P was constructed to delete nucleotides 6486828 to 6487525 of the *tgd057* locus on chrXI annotated as TGME49_015980. The *HXGPRT* minigene cassette was fused between an 800-bp 5′ *tgd057* genomic targeting flank and a 1,259-bp 3′ *tgd057* genomic targeting flank amplified from Pru genomic DNA.

Plasmid pGRA4X was constructed to insert the coding region of *GRA4* into the *UPRT* locus under the control of the *UPRT* 5′ transcribed, untranslated region (5′UTR). Targeted insertion of the pGRA4X cassette deleted nucleotides 2709350 to 2713372 of the coding region of the *UPRT* chromosomal locus on chrXI annotated as TGME49_112480. The *GRA4* coding region (plus 12 bp 5′ of the ATG) and 635 bp of the *GRA4* 3′UTR (nucleotides 1579415 to 1581100 on ChrXI) was amplified from Pru genomic DNA and inserted between the 5′ *UPRT* target flank and the *HXGPRT* marker of plasmid pΔUPRP.

Plasmid pGRA6X was constructed to insert the coding region of *GRA6* into the *UPRT* locus under the control of the *UPRT* 5′UTR. Targeted insertion of the pGRA6X cassette deleted nucleotides 2709350 to 2713372 of the coding region of the *UPRT* chromosomal locus on chrXI annotated as TGME49_112480. The *GRA6* coding region (plus 15 bp 5′ of the ATG) and 542 bp of the *GRA6* 3′UTR (nucleotides 7214586 to 7215818 on ChrX) was amplified from Pru genomic DNA and inserted between the 5′ *UPRT* target flank and the *HXGPRT* marker of plasmid pΔUPRP.

Culture conditions and strains. All parasite strains were continuously maintained *in vitro* by serial passage in Eagle modified essential medium supplemented with 1% fetal bovine serum in diploid human foreskin fibroblasts (HFF) at 36°C (26). Pyrimidine auxotrophs were supplemented with uracil (250 μM). The parental Pru strain (Δ*hxgprt*) was previously made transgenic for green fluorescent protein (GFP) under the control of the *LDH2* bradyzoite stage-specific promoter and was designated BSG-4 (60). The *T. gondii* strains used and developed in the present study are shown in Table 1. We previously reported the RHΔ*ku80*Δ*hxgprt* strain (26).

Transformation, selection, and gene deletion verification strategy. Electroporations were performed using a model BTX600 electroporator and previously described methods (26). All transfected plasmids were linearized 5′ of the 5′ target DNA flank prior to transfection using unique restriction enzyme sites designed into the targeting plasmids. Forward selections to integrate the pmini-HXGPRT selectable marker were performed in mycophenolic acid (MPA; 25 μg/ml) and xanthine (50 μg/ml) (16, 26). Negative selections to excise *HXGPRT* were performed in 6-thioxanthine (6TX) (200 μg/ml) (23, 26). Negative selections using the cytosine deaminase (CD) selectable marker were performed in

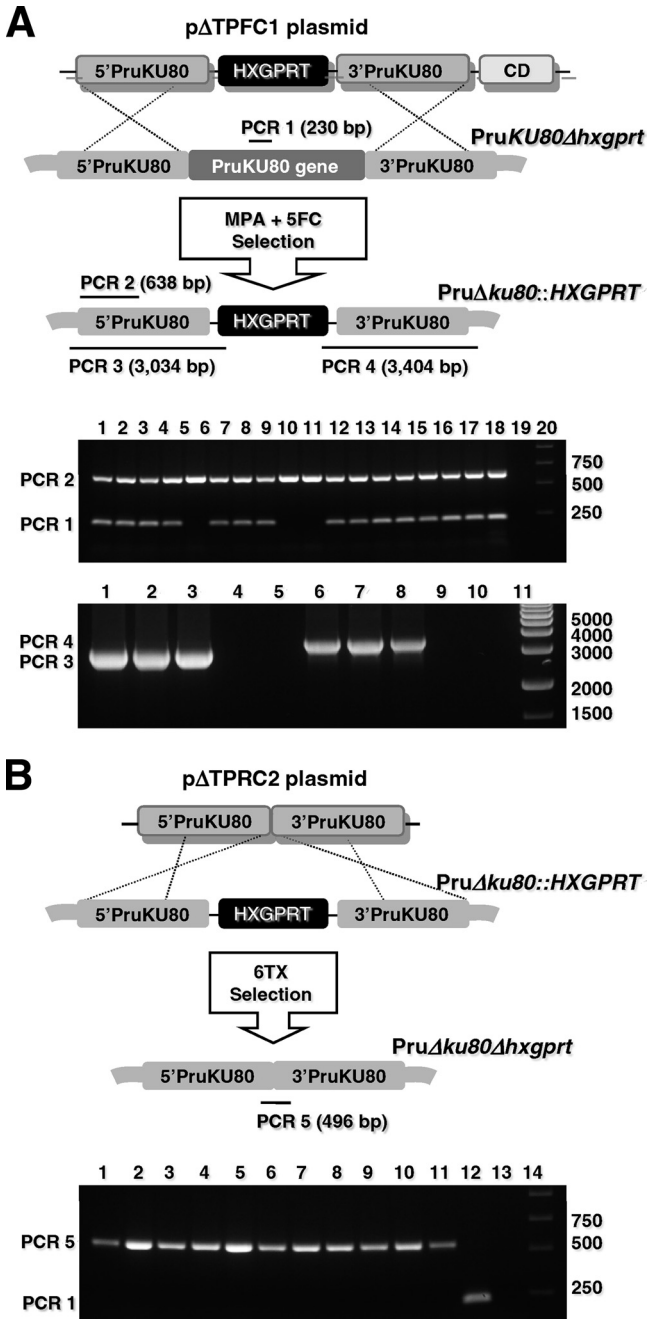

FIG. 1. Construction of the type II Δ*ku80* Δ*hxgprt* genetic background. (A) Strategy for disrupting the *KU80* gene in the parental Pru strain via integration of the *HXGPRT* marker. Approximate locations of PCR products using primer pairs to verify the genotype at the *KU80* locus (not to scale) and the expected PCR product sizes are shown. (Top agarose gel panel) PCR 1 and PCR 2 products: 17 randomly selected clones isolated after selection (lanes 1 to 17), parental Pru (lane 18), no template (lane 19), DNA size ladder (lane 20). Clones in lanes 5, 9, and 10 appear negative for PCR 1 showing deletion of the *KU80* gene. (Bottom agarose gel panel) PCR 3: clones from lanes 5, 9, and 10 (lanes 1 to 3), parental Pru (lane 4), no template (lane 5); PCR 4: clones from lanes 5, 9, and 10 (lanes 6 to 8), parental Pru (lane 9), no template (lane 10). DNA size ladder (lane 11). A targeted *KU80* knockout is positive for the PCR 2, PCR 3, and PCR 4 products and negative for the PCR 1 product. Genotypes with an intact *KU80* locus are positive for PCR 1 and PCR 2 and negative for PCR 3 and PCR 4. (B) Excision of the *HXGPRT* marker from the *KU80* locus in the Pru*Δku80*::*HXGPRT* strain. The strategy for excision of *HXGPRT* is depicted with negative selection in 6TX after transfection with plasmid pΔTPRC2. Approximate locations of PCR products using primer pairs to verify genotype are depicted (not to scale). The expected PCR product sizes are shown for a positive result. (Agarose gel panel) PCR 1 and PCR 5 products: 11 clones isolated after 6TX selection (lanes 1 to 11), parental Pru (lane 12), parental Pru*Δku80*::*HXGPRT* (lane 13), DNA size ladder (lane 14). The Pru*Δku80Δhxgprt* strain is positive for PCR 5 and negative for PCR 1 (lanes 1 to 11), the parental Pru strain is positive for PCR 1 and negative for PCR 5 (lane 12), and the parental Pru*Δku80*::*HXGPRT* strain is negative for PCR 1 (496-bp product) and PCR 5 (lane 13).

5-fluorocytosine (5FC; 50 μM) (22, 26). Negative selections to delete UPRT were performed in 5 μM 5-fluorodeoxyuridine (FUDR) (17). After transfection, parasites were allowed to replicate for 24 h without selection to allow replication and ramp up homologous recombination, and then selections were launched and continuously maintained through verification steps of cloned isolates. The strategy for verification of mutant strains was previously described (23, 26).

Genomic DNA isolation and PCR. Genomic DNA purifications used a DNA blood minikit (Qiagen) and were performed with a Qiacube automated robotic work station (Qiagen). PCR products were amplified using a 1:1 mixture of *Taq* DNA polymerase and an Expand long-template PCR (Roche).

Determination of gene replacement frequencies and statistical analysis. PFU assays were used to determine gene replacement frequencies. Three replicate PFU flasks were prepared for each titration point and selection condition. A Student *t* test analysis was used to calculate the standard error of the mean (SEM). PFU assays were performed at various times after transfection to determine the gene replacement frequency at the *UPRT* locus based on the fraction of parasites that had dual resistance to MPA and FUDR compared to the fraction of parasites that were resistant only to MPA (26). PFU assays were performed at various times after transfection to determine the gene replacement frequency at the *OPRT* locus based on the fraction of parasites that exhibited resistance to MPA and grew with uracil supplementation compared to the fraction of parasites that were resistant to MPA without uracil supplementation (25).

Determination of the replication rate of mutant strains *in vitro*. The intracellular growth rate of various type II strains was measured in HFFs in a 45-h growth assay using previously described methods (24). Briefly, freshly lysed tachyzoites were Nuclepore filtered to isolate individual tachyzoites that were used to infect HFF monolayers at a multiplicity of infection of ~0.1. After 1 h of invasion, the culture was vigorously washed four times in phosphate-buffered saline (PBS) to remove extracellular tachyzoites (verified by microscopy). Cultures were then returned to growth medium, and the number of parasites per vacuole was scored from at least 50 vacuoles per sample at 45 h postinfection. Cultures were prepared in duplicate, and the growth assay was repeated twice. The data samples were subjected to a Student *t* test and are represented as the means (parasites per vacuole) ± the SEM. Differences in parasites per vacuole were compared for parental and mutant strains matched for the presence or absence of HXGPRT. A P value of <0.05 was considered significant.

Mice. Female 7- to 9-week-old C57BL/6 (H-2K^b), CBA (H-2K^k), and BALB/c (H-2L^d) mice were purchased from Jackson laboratories (Bar Harbor, ME) and maintained at the Dartmouth-Hitchcock Medical Center mouse facility. All mice were cared for and handled according to Animal Care and Use Program of Dartmouth College using National Institutes of Health (NIH)-approved institutional animal care and use committee guidelines. Groups of mice (as indicated) were infected by oral gavage with 10 cysts or were infected by intraperitoneal injection with 0.2 ml (200 tachyzoites) of various Pru genotypes in PBS. Each tachyzoite preparation was subjected to a PFU assay to determine viability. All mice infected with tachyzoites received 130 to 252 PFU. Infected mice were then monitored daily for wellness.

Cyst isolation, visualization, enumeration, and size determination. Brains from mice inoculated with various genotypes of the Pru background were harvested and homogenized by using a Dounce homogenizer in 2 ml of sterile PBS (30). All cyst counts were performed immediately after the isolation of brain homogenates. In most experiments, 20 slides (10%) of each brain were scored for cysts, and any deviation from this counting scheme was performed only in cases when cyst numbers were low and additional slides were scored. Cysts were scored under an inverted fluorescence phase-contrast microscope (Olympus CKX41) to count GFP-positive (GFP$^+$) cysts at a magnification of ×150, which provided the highest sensitivity for the detection of GFP$^+$ cysts. Average cyst size was mea-

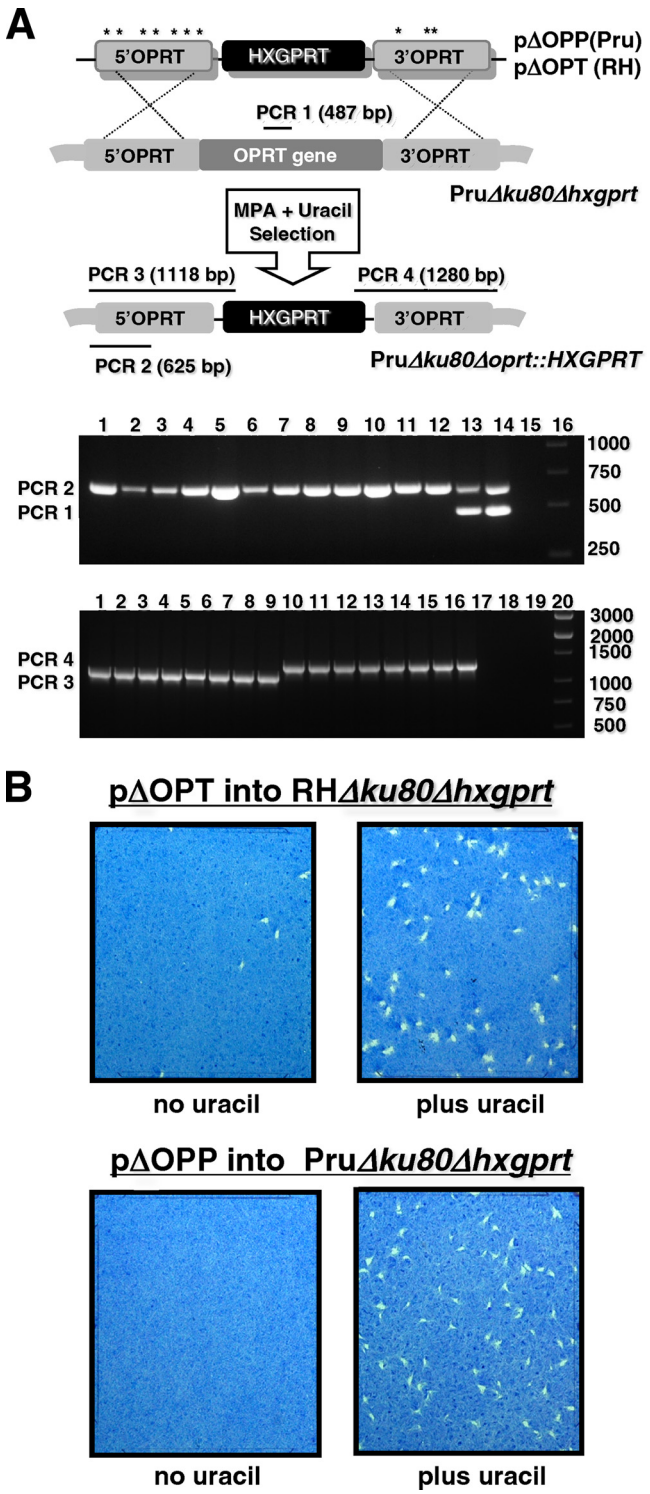

FIG. 2. Targeted gene replacement at the orotate phosphoribosyltransferase (*OPRT*) locus. (A) Strategy for disruption of *OPRT* by double-crossover homologous recombination in type II strain Pru*Δku80Δhxgprt* using plasmid pΔOPP and in type I strain RH*Δku80Δhxgprt* using plasmid pΔOPT. Compared to plasmid pΔOPP, plasmid pΔOPT contains seven single-nucleotide polymorphisms (indicated by "*") in the 5′ targeting DNA flank and three nucleotide polymorphisms in the 3′ targeting DNA flank. The PCR strategy for genotype verification of deletion of *OPRT* is depicted (not to scale). The expected PCR product sizes are shown for a positive result. (Top agarose gel panel) PCR 1 and PCR 2 products: 6 clones isolated after targeting type I *OPRT* deletion (lanes 1 to 6), 6 clones isolated after targeting type II *OPRT* deletion (lanes 7 to 12), parental type I RH*Δku80Δhxgprt* (lane 13), parental type II Pru*Δku80Δhxgprt* (lane 14), no template (lane 15) DNA size ladder (lane 16). All six type I clones and all six type II clones appear to be *OPRT* knockouts (PCR 1 negative and PCR 2 positive). Type I and type II clones were evaluated in PCR 3 and PCR 4 to verify integration of *HXGPRT* at the deleted *OPRT* locus. (Bottom agarose gel panel) PCR 3 products: type I clones (lanes 1 to 4), type II clones (lanes 5 to 8); PCR 4 products: type I clones (lanes 9 to 12), type II clones (lanes 13 to 16); PCR 3 and PCR 4 on parental type I RH*Δku80Δhxgprt* (lane 17), PCR 3 and PCR 4 on parental type II Pru*Δku80Δhxgprt* (lane 18), PCR 3 and PCR 4 using no template (lane 19), DNA size ladder (lane 20). (B) PFU assays were performed at various times after transfection of pΔOPT in the type I RH*Δku80Δhxgprt* (top) or after transfection of plasmid pΔOPP into the type II Pru*Δku80Δhxgprt* (bottom) to determine the gene replacement frequency at the *OPRT* locus based on the fraction of parasites that exhibited resistance to MPA and grew with uracil supplementation compared to the fraction of parasites that were resistant to MPA without uracil supplementation (Table 2). The PFU assays shown were sampled 25 days posttransfection with or without uracil. All PFU assays contained MPA selection medium.

sured as a relative unit of diameter. Average cyst size was determined at a magnification of ×150 by measuring bradyzoite diameter units (BDU). BDU were determined for each randomly selected cyst by counting the number of GFP^+ bradyzoites residing in a direct line from one edge of the cyst wall to the opposite edge of the cyst wall at the maximum point of the cyst diameter. BDU were determined for 25 randomly selected cysts from each mouse brain tissue sample. At least five mice were used to determine BDU for each parasite strain tested. Cyst data samples were subjected to a Student *t* test and are represented as means ± the SEM. Differences in cyst burdens between groups of infected mice were significant if the *P* value was <0.05. Cysts were also evaluated using confocal microscopy. Images were acquired using a Zeiss LSM 510 Meta laser scanning confocal microscope equipped with a 20× Plan Apo NA 0.75 objective lens (Carl Zeiss Microimaging, Thornwood, NY). Confocal settings were set to 1 Airy unit (1.8-μm optical section). A zoom setting of six generated a pixel size of 0.15 by 0.15 μm. LSM 510 software version 3.2 was used.

RESULTS

Generation of *T. gondii* strains Pru*Δku80*::*HXGPRT* and Pru*Δku80Δhxgprt*. Alignments of the predicted type I (26) and type II (TGME49_112510, 583.m05492 [www.toxodb.org] version 4.0) *KU80* loci revealed frequent strain specific nucleotide polymorphisms. Plasmid pΔTPR1 was developed to functionally delete the type II *KU80* gene. Multiple independent transfections of various type II strains, selections, and screens of more than ~800 MPA resistant clones failed to identify a targeted *KU80* knockout in any type II strain.

We constructed plasmid pΔTPFC1 with the cytosine deaminase (*CD*) gene inserted 3′ of the 3′ *KU80* target DNA flank (Fig. 1A). Inclusion of the *CD* gene provided a more robust selection strategy for double crossovers at the *KU80* locus by using negative selection to eliminate transformants that still retained expression of CD by growth of the transfected parasite population in 5-fluorocytosine (Fig. 1A). After continued attempts using the *CD* negative selection strategy, we detected a low frequency of *KU80* knockout clones (Pru*Δku80*::*HXGPRT*) that were positive for PCR 2 and were negative for PCR 1 that probes for the presence of the targeted deletion in the *KU80* gene (Fig. 1A, lanes 5, 9, and 10, top gel panel). Three PCR 1-negative clones were then validated as

TABLE 2. Gene replacement frequency at the *OPRT* locus in type I and type II *KU80* knockouts

Transfected strain	Plasmid[a]	Day assayed	Gene replacement (%) at the *OPRT* locus	
			Expt 1	Expt 2
RHΔ*ku80*Δ*hxgprt*	pΔOPT	18	92.1	93.0
RHΔ*ku80*Δ*hxgprt*	pΔOPT	25	91.4	94.3
PruΔ*ku80*Δ*hxgprt*	pΔOPP	18	98.8	99.3
PruΔ*ku80*Δ*hxgprt*	pΔOPP	25	99.7	99.8
PruΔ*ku80*Δ*hxgprt*	pΔOPT	18	13.2	12.4
PruΔ*ku80*Δ*hxgprt*	pΔOPT	25	10.6	14.9

[a] pΔOPT is derived from type I RH, and pΔOPP is derived from type II Pru.

TABLE 3. Gene replacement frequency at the *UPRT* locus

Transfected strain	Plasmid	Day assayed	Gene replacement (%) at the *UPRT* locus	
			Expt 1	Expt 2
PruΔ*hxgprt*	pΔUPRP	25	0.03	0.00
PruΔ*hxgprt*	pΔUPRP	32	0.08	0.00
PruΔ*ku80*Δ*hxgprt*	pΔUPRP	10	3.74	2.90
PruΔ*ku80*Δ*hxgprt*	pΔUPRP	18	46.7	55.4
PruΔ*ku80*Δ*hxgprt*	pΔUPRP	25	75.9	82.1
PruΔ*ku80*Δ*hxgprt*	pΔUPRP	32	97.1	99.2

targeted *KU80* knockouts using PCR 3 and PCR 4 to demonstrate precise 5′ and 3′ integration of *HXGPRT* at the deleted *KU80* locus (Fig. 1A, bottom gel panel). To delete the *HXGPRT* marker from the PruΔ*ku80*::*HXGPRT* strain, two clones were transfected with plasmid pΔTPRC2, which is identical to plasmid pΔTPR1 but lacks the *HXGPRT* gene (Fig. 1B). 6TX-resistant parasite clones were obtained, and these clones uniformly exhibited the genotype Δ*ku80* Δ*hxgprt* based on PCR analysis using PCR 1 and PCR 5 that was designed to span the deleted region of *KU80* and to demonstrate the targeted deletion of the 2-kb *HXGPRT* marker (Fig. 1B).

Influence of DNA sequence homology on gene replacement frequency at the *OPRT* locus. Disruption of *de novo* pyrimidine synthesis induces uracil auxotrophy (23, 24). Here, the *OPRT* locus was targeted for deletion to induce uracil auxotrophy as a phenotype. Type II *OPRT* deletion was targeted using plasmid pΔOPP and type I OPRT deletion was targeted using plasmid pΔOPT (Fig. 2A). *OPRT* knockouts were obtained in type I and type II backgrounds based on the identification of clones that were positive for PCR 2 and negative for PCR 1 that probes for the presence of the targeted deletion in the *OPRT* gene (Fig. 2A, top gel panel). Using PCR 3 and PCR 4, four of these clones from each strain type were then shown to be targeted *OPRT* deletions based on precise 5′ and 3′ integration of the *HXGPRT* marker at the *OPRT* locus (Fig. 2A, bottom gel panel).

The efficiency of gene targeting at the *OPRT* locus in the type I versus the type II Δ*ku80* Δ*hxgprt* strain was measured using target DNA flanks with a strain-specific DNA homology of 100% (Fig. 2A) (Table 2). PFU assays performed on the MPA-selected population of parasites at 18 and again at 25 days posttransfection of the targeting plasmids revealed that targeted disruption of *OPRT* created the uracil auxotroph phenotype at a high frequency in both the type I and the type II Δ*ku80* Δ*hxgprt* strains (Fig. 2B). The gene targeting frequency at the *OPRT* locus was found to be slightly higher in the type II strain PruΔ*ku80*Δ*hxgprt* (99.8% ± 0.1%) compared to the type I strain RHΔ*ku80*Δ*hxgprt* (92.9% ± 1.5%) (Table 2).

Naturally occurring nucleotide polymorphisms present within the 5′ and 3′ noncoding DNA between type I and type II strains enabled a test of homology requirements necessary for efficient gene targeting at the *OPRT* locus in *T. gondii* (Fig. 2A). These nucleotide polymorphisms divided the 5′ target flank into segments of 94, 162, 53, 127, 39, 240, 88, and 247 bp of homology and the 3′ target flank into segments of 530, 22, 359, and 208 bp of homology (sequence alignments between type I and type II *OPRT* are not shown). Type I targeting plasmid pΔOPT with 7 nucleotide mismatches in the 5′ target DNA flank and 3 mismatches in the 3′ target DNA flank relative to type II was inefficient in targeting gene deletion at the type II *OPRT* locus (Table 2).

Targeted disruption of the key enzymes of the pyrimidine salvage pathway. Disruption of *UPRT* was used to measure gene replacement efficiency in strain PruΔ*ku80*Δ*hxgprt* (26). The frequency of gene replacement at the *UPRT* locus was determined at different time points after transfection of plasmid pΔUPRP by plating equal numbers of parasites either in MPA or in MPA plus FUDR selection. The nonreverting PruΔ*ku80*Δ*uprt*::*HXGPRT* genotype was also confirmed in several MPA resistant clones (data not shown). The frequency of gene replacement at the *UPRT* locus in strain PruΔ*ku80*Δ*hxgprt* was found to be only 3.3% ± 0.4% at 10 days posttransfection, but this frequency steadily increased to 98.2% ± 1.1% by day 32 posttransfection (Table 3). In contrast, the gene replacement efficiency in the parental Pru strain was <0.10% at 32 days postinfection (Table 3).

It is currently unknown whether the two critical enzymes of the pyrimidine salvage pathway (23) (UPRT and uridine phosphorylase [UP]) are required for cyst development and latent *T. gondii* infection. To complete a genetic dissection of the major pyrimidine salvage activities in the type II *T. gondii* and to assess the potential role of the salvage pathway in cyst development, we deleted the *UP* gene using plasmid pΔUPP (data not shown) (Table 1). We found that 23 of 24 randomly selected MPA-resistant clones (96%) had the *UP* gene deleted.

Efficient targeted excision of the *HXGPRT* selectable marker from PruΔ*ku80* mutant strains. *HXGPRT* was targeted for deletion from the *OPRT* locus in strain PruΔ*ku80*Δ*oprt*::*HXGPRT* using plasmid pΔOPPC and negative selection in 6TX. Strain PruΔ*ku80*Δ*oprt* was easily isolated and validated by PCR analysis (data not shown) (Table 1).

PruΔ*ku80*Δ*hxgprt* stably maintains the ability to develop cysts and chronic infection in mice. We observed no significant difference ($P = 0.20$) between the *in vitro* intracellular replication rates of strain PruΔ*ku80*Δ*hxgprt* (14.2 ± 0.50 parasites/vacuole) compared to the parental Pru strain (15.0 ± 0.15 parasites/vacuole) (Table 4). The type II strain PruΔ*ku80*Δ*hxgprt* stably maintained the ability to develop brain tissue cyst burdens in mice after more than 16 months of continuous *in vitro* culture. Brain tissue cysts obtained from mice infected with the strain PruΔ*ku80*Δ*hxgprt* revealed a cyst wall structure (Fig. 3A), as well as the expected bradyzoite stage-specific expres-

TABLE 4. Intracellular replication rate of selected strains used in this study

Strain (reference)	Mean no. of parasites per vacuole[a] ± SEM	*P* (compared to the control strain)[b]		
		P	Significance	Control strain genotype
PruΔ*ku80*Δ*gra4*::*HXGPRT*	14.1 ± 0.48	0.74	NS	Δ*ku80*::*HXGPRT*
PruΔ*ku80*Δ*gra6*::*HXGPRT*	13.9 ± 0.29	1	NS	Δ*ku80*::*HXGPRT*
PruΔ*ku80*Δ*gra6*Δ*gra4*::*HXGPRT*	13.2 ± 0.14	0.09	NS	Δ*ku80*::*HXGPRT*
PruΔ*ku80*Δ*uprt*::*HXGPRT*	14.2 ± 0.13	0.33	NS	Δ*ku80*::*HXGPRT*
PruΔ*ku80*Δ*tgd057*::*HXGPRT*	15.2 ± 0.31	0.02	S	Δ*ku80*::*HXGPRT*
PruΔ*ku80*Δ*rop4/7*::*HXGPRT*	14.9 ± 0.20	0.03	S	Δ*ku80*::*HXGPRT*
PruΔ*ku80*::*HXGPRT*	13.9 ± 0.31		ND	
PruΔ*hxgprt* (parental) (60)	15.0 ± 0.17		ND	
PruΔ*ku80*Δ*hxgprt*	14.2 ± 0.57	0.20	NS	Δ*hxgprt* (parental)
PruΔ*ku80*Δ*gra4*Δ*hxgprt*	14.5 ± 0.36	0.70	NS	Δ*ku80* Δ*hxgprt*
PruΔ*ku80*Δ*gra6*Δ*hxgprt*	13.8 ± 0.23	0.51	NS	Δ*ku80* Δ*hxgprt*
PruΔ*ku80*Δ*gra6*Δ*gra4*Δ*hxgprt*	13.5 ± 0.36	0.36	NS	Δ*ku80* Δ*hxgprt*

[a] Parasites per vacuole were scored after 45 h of intracellular replication.
[b] To determine the *P* value, strains were matched for the presence or absence of *HXGPRT*. S, significant; NS, not significant; ND, not determined.

sion of GFP (Fig. 3B and C) (60). In contrast, GFP expression was not detected in strain PruΔ*ku80*Δ*hxgprt* during *in vitro* culture of the tachyzoite stages (data not shown). In addition, brain cyst burdens in C57BL/6 mice at 3 weeks postinfection with strain PruΔ*ku80*Δ*hxgprt* (942 ± 184) were essentially identical ($P = 0.70$) to the brain cyst burdens observed after infection with the parental Pru strain (1,065 ± 262) (Fig. 3D). Furthermore, cyst sizes in strain PruΔ*ku80*Δ*hxgprt* (13.0 ± 0.46 BDU) were essentially identical ($P = 0.63$) to the cyst sizes measured in the parental Pru strain (13.3 ± 0.47 BDU) (Fig.

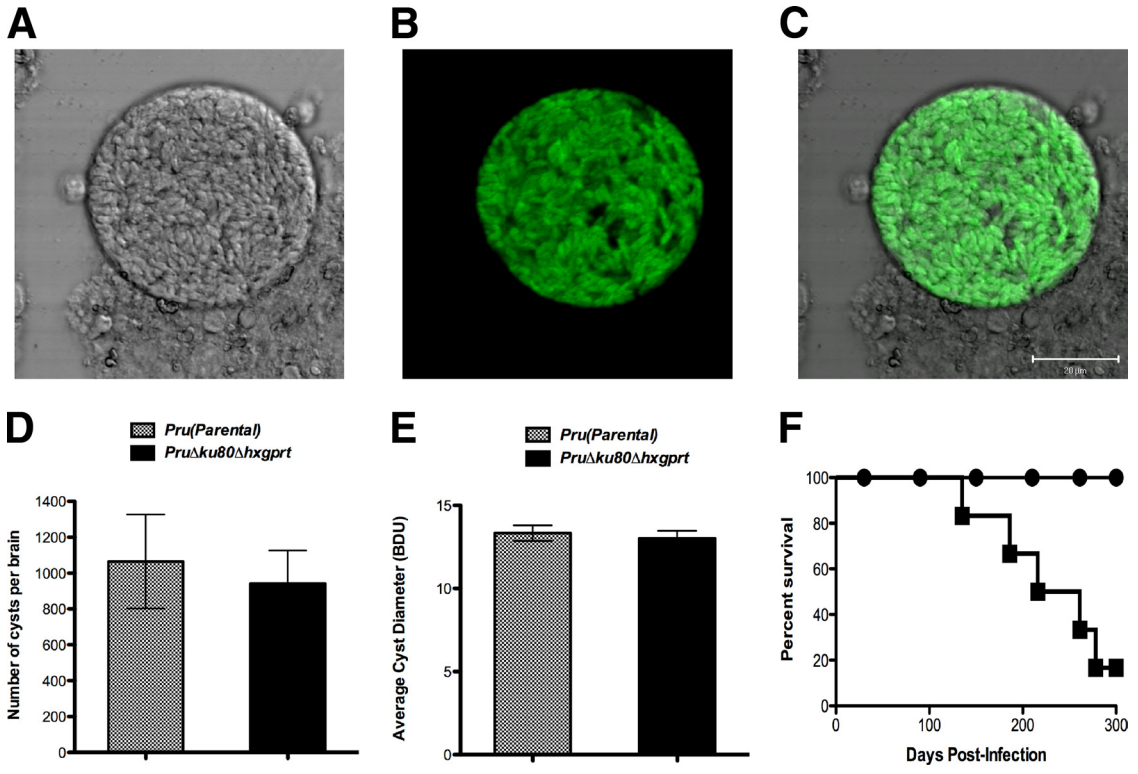

FIG. 3. The PruΔ*ku80*Δ*hxgprt* strain elicits GFP$^+$ cysts and chronic and/or latent infection in genetically susceptible C57BL/6 mice. (A to E) C57BL/6 mice were infected by intraperitoneal inoculation of 200 of the tachyzoites of PruΔ*ku80*Δ*hxgprt* strain or the parental Pru strain. (A, B, and C) An example of a cyst observed at 5 weeks postinfection of C57BL/6 mice with strain PruΔ*ku80*Δ*hxgprt*. (A) Bright-field laser confocal microscopy with light collected from a 1.8-μm-thick section. (B) GFP$^+$ fluorescence from the same sample shown in panel A. (C) Merge of panels A and B. (D) Brain cyst burdens were measured in the parental Pru strain and the PruΔ*ku80*Δ*hxgprt* strain at 3 weeks postinfection of C57BL/6 mice. (E) The average size of brain cysts was determined in the parental Pru strain and the PruΔ*ku80*Δ*hxgprt* strain at 3 weeks postinfection of C57BL/6 mice as a relative measure of cyst diameter (BDU [see Materials and Methods]). (F) C57BL/6 mice were perorally infected with 10 cysts of the PruΔ*ku80*Δ*hxgprt* strain. A survival curve of C57BL/6 mice ($n = 6$) infected perorally with 10 brain cysts of strain PruΔ*ku80*Δ*hxgprt* (solid squares), or uninfected mice ($n = 4$) inoculated with PBS (solid circles).

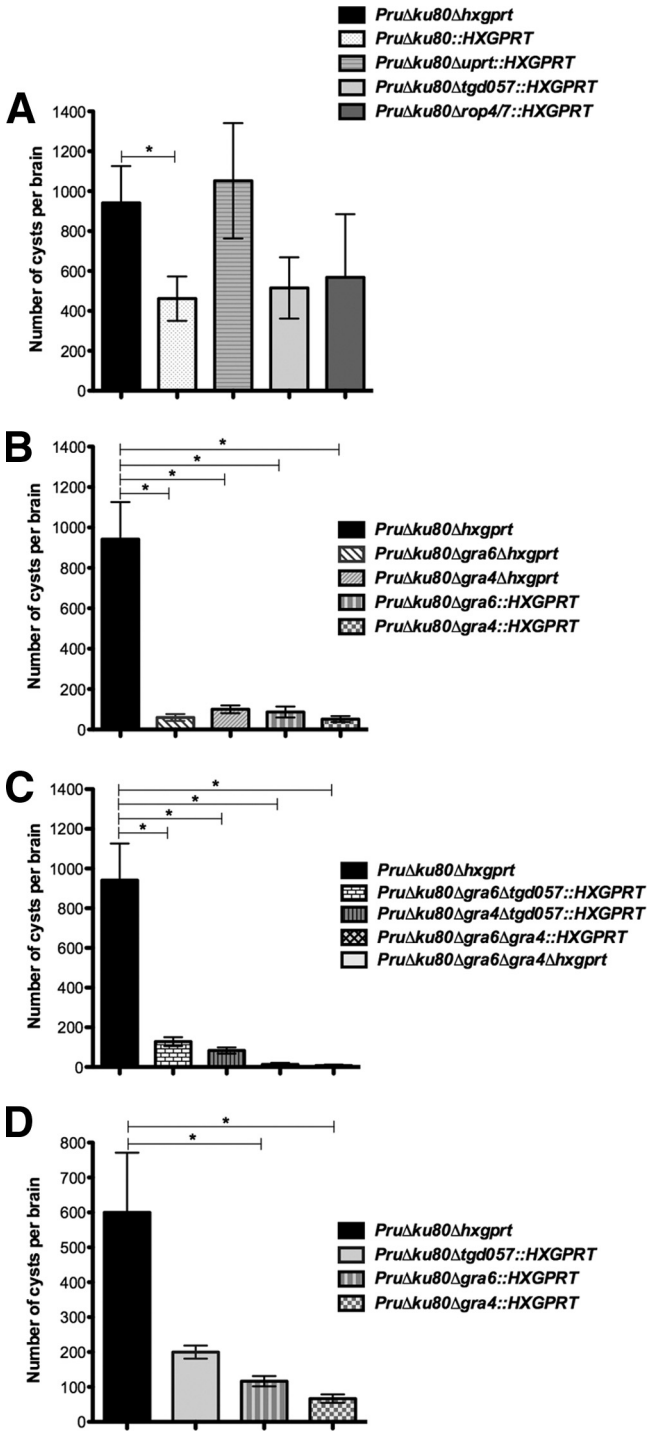

FIG. 4. Brain cyst burdens measured at 3 weeks postinfection. C57BL/6 or CBA mice were infected by intraperitoneal inoculation of 200 tachyzoites of mutant or parental strains. (A, B, and C) Brain cyst burdens in C57BL/6 mice. (A) Cyst burdens were measured at 3 weeks postinfection of C57BL/6 mice infected with the strain genotypes Δ*ku80*::*HXGPRT* (6 mice), Δ*ku80* Δ*hxgprt* (6 mice), Δ*ku80* Δ*uprt*::*HXGPRT* (5 mice), Δ*ku80* Δ*tgd057*::*HXGPRT* (6 mice), and Δ*ku80* Δ*rop4*/*7*::*HXGPRT* (6 mice). (B) Cyst burdens were measured at 3 weeks postinfection of C57BL/6 mice infected with the strain genotypes Δ*ku80* Δ*hxgprt* (6 mice), Δ*ku80* Δ*gra4*::*HXGPRT* (6 mice), Δ*ku80* Δ*gra6*::*HXGPRT* (6 mice), Δ*ku80* Δ*gra4* Δ*hxgprt* (4 mice), and Δ*ku80* Δ*gra6* Δ*hxgprt* (4 mice). (C) Cyst burdens were measured at 3 weeks postinfection of C57BL/6 mice infected with the strain genotypes Δ*ku80* Δ*hxgprt* (6 mice), Δ*ku80* Δ*gra4* Δ*tgd057*::*HXGPRT* (6 mice), Δ*ku80* Δ*gra6* Δ*tgd057*::*HXGPRT* (6 mice), Δ*ku80* Δ*gra6* Δ*gra4*::*HXGPRT* (6 mice), and Δ*ku80* Δ*gra6* Δ*gra4* Δ*hxgprt* (4 mice). (D) Brain cyst burdens in CBA mice. Cyst burdens were measured at 3 weeks postinfection of CBA mice infected with strain genotypes Δ*ku80* Δ*hxgprt* (6 mice), Δ*ku80* Δ*gra4*::*HXGPRT* (6 mice), Δ*ku80* Δ*gra6*::*HXGPRT* (6 mice), and Δ*ku80* Δ*tgd057*::*HXGPRT* (4 mice). Cyst data samples were subjected to a Student *t* test and are represented as the means ± the SEM. Cyst burdens determined in mutant strains were compared to cyst burdens in the parental Δ*ku80* Δ*hxgprt* strain to establish significance ($P < 0.05$).

3E). Finally, peroral infection of the genetically susceptible C57BL/6 background with 10 brain cysts of strain Pru*Δku80Δhxgprt* caused an acute infection with morbidity, and infected mice recovered and then developed the expected chronic infection that eventually led to mortality (Fig. 3F). Deletion of the *KU80* gene in strain Pru*Δku80Δhxgprt* did not lead to any significant defects in regard to the intracellular growth rate, the development of brain cyst burdens, the cyst size, or the establishment of a chronic or latent infection.

Targeted deletions at the *GRA4*, *GRA6*, *ROP4*/*7*, and *tgd057* loci. To assess the interplay of host response and cyst development, targeted deletions were developed at the four gene loci known to encode $CD8^+$ T cell epitopes that elicit corresponding antigen-specific $CD8^+$ T cell populations during *T. gondii* infection. Targeting plasmids pΔGRA4P, pΔGRA6P, pΔROP4/7P, and pΔTGD057P were used to develop mutant strains with deletions of the *GRA4*, *GRA6*, *ROP4*/*7*, or *tgd057* loci. Plasmids pΔGRA4PC and pΔGRA6PC were then used to target the removal of *HXGPRT* from the disrupted *GRA4* and *GRA6* loci in 6TX-negative selections. Finally, the *GRA4* and *GRA6* strains with *HXGPRT* deleted were used to develop several mutant strains with targeted deletion of two genetic loci (Δ*ku80* Δ*gra6* Δ*gra4*::*HXGPRT*, Δ*ku80* Δ*gra4* Δ*tgd057*::*HXGPRT*, and Δ*ku80* Δ*gra6* Δ*tgd057*::*HXGPRT*) (Table 1).

Determination of the replication rate of mutant strains *in vitro*. None of the mutant strains examined exhibited any significant decrease in their intracellular growth rate in a 45 h growth assay (parasites per vacuole) compared to the control strain matched for the presence or absence of *HXGPRT* (Table 4). Two of the mutant strains, Δ*ku80* Δ*tgd057*::*HXGPRT* ($P = 0.020$) and Δ*ku80* Δ*rop4*/*7*::*HXGPRT* ($P = 0.032$), were found to exhibit a significant increase in the number of parasites per vacuole in the 45-h *in vitro* growth assay.

Measurement of brain tissue cyst burdens in mice infected with mutant strains. Cyst development was examined in the genetically susceptible C57BL/6 murine background that exhibits higher cyst burdens, reactivation, and chronic infection compared to the genetically resistant BALB/c murine background (30, 45, 56). Cyst burdens measured at 3 weeks postinfection of C57BL/6 mice were 462 ± 111 for the Pru*Δku80*::*HXGPRT* strain and 942 ± 184 for the Pru*Δku80Δhxgprt* strain (Fig. 4A; $P = 0.0499$). Nonetheless, all of the knockouts reported in the present study were developed in the Pru*Δku80Δhxgprt* parent strain that is normal in regard to intracellular replication rate, cyst development, and cyst burdens (Fig. 3). The mutant strains developed in the

Pru*Δku80Δhxgprt* parent share the identical disrupted *KU80* locus and differ only in regard to the presence of *HXGPRT* that is inserted at the gene locus targeted for deletion. Consequently, several gene knockouts developed in the Pru*Δku80Δhxgprt* strain using *HXGPRT* selection were subsequently deleted of *HXGPRT* to allow more optimal assessment of phenotypes in comparison to the parental Pru*Δku80Δhxgprt* strain.

Several mutant strains, including Pru*Δku80Δup*::*hxgprt* (data not shown), Pru*Δku80Δuprt*::*hxgprt* ($P = 0.75$), Pru *Δku80Δrop4/7*::*hxgprt* ($P = 0.33$), and Pru*Δku80Δtgd057*::*hxgprt* ($P = 0.11$), exhibited no significant difference in cyst burdens compared to the parental Pru*Δku80Δhxgprt* strain at 3 weeks postinfection (Fig. 4A). In contrast, at 3 weeks postinfection of C57BL/6 mice, a 91% reduction ($P = 0.0010$) in cyst burden was observed in the Δ*gra6* mutant with *HXGPRT* (Δ*ku80* Δ*gra6*::*HXGPRT*) and a 91% reduction ($P = 0.0010$) in cyst burden was observed in the Δ*gra4* mutant with *HXGPRT* (Δ*ku80* Δ*gra4*::*HXGPRT*) (Fig. 4B). Similarly, a 93% reduction ($P = 0.0051$) in cyst burden was observed in the Δ*gra6* mutant with *HXGPRT* deleted (Δ*ku80* Δ*gra6* Δ*hxgprt*) and an 89% reduction ($P = 0.0066$) in cyst burden was observed in the Δ*gra4* mutant with *HXGPRT* deleted (Δ*ku80* Δ*gra4* Δ*hxgprt*) (Fig. 4B). Double mutants involving the *GRA4* and/or the *GRA6* loci were also examined for cyst development in C57BL/6 mice. Although the Pru*Δku80Δgra4Δtgd057*::*HXGPRT* (91% reduction; $P = 0.0009$) and Pru*Δku80* Δ*gra6*Δ*tgd057*::*HXGPRT* (86%; $P = 0.0032$) mutant strains revealed similar reductions in cyst burden (Fig. 4C) compared to the Δ*gra4* and Δ*gra6* single mutants with or without the *HXGPRT* marker (Fig. 4B), the double-mutant strain Pru*Δku80*Δ*gra6*Δ*gra4*::*HXGPRT* revealed a markedly more severe defect in cyst burdens at 3 weeks postinfection (99% reduction; $P = 0.0005$) (Fig. 4C). This more significant defect in cyst burden in the Δ*ku80* Δ*gra6* Δ*gra4*::*hxgprt* double mutant was then verified by construction of the Δ*ku80* Δ*gra6* Δ*gra4* Δ*hxgprt* strain that exhibited a 99.8% reduction ($P = 0.0037$) in cyst burden (Fig. 4C). Collectively, these results demonstrate a significant defect in the development of brain cyst burdens in mutant strains with *GRA4* and/or *GRA6* deleted in C57BL/6 mice.

We also measured cyst burdens in the CBA murine (H-2K^k) background because the four currently characterized CD8$^+$ T cell epitopes encoded by the *GRA4*, *GRA6*, *ROP7*, and *tgd057* genes are not recognized by the H-2K^k-restricted CBA background. In the CBA murine background a 77% reduction ($P = 0.018$) in cyst burden was observed in the Δ*gra6* mutant and an 87% reduction ($P = 0.011$) in cyst burden was observed in the Δ*gra4* mutant at 3 weeks postinfection (Fig. 4D). In contrast, no significant difference in cyst burden was observed in the Δ*tgd057* mutant ($P = 0.099$).

In addition, the cyst burdens for many of the mutant strains were also measured at 5 weeks postinfection of C57BL/6 mice. The Pru*Δku80*::*HXGPRT* ($P = 0.28$), Pru*Δku80Δuprt*::*HXGPRT* ($P = 0.25$), and Pru*Δku80Δtgd057*::*HXGPRT* ($P = 0.90$) strains exhibited no significant difference in cyst burdens compared to the Pru*Δku80Δhxgprt* strain at 5 weeks postinfection (Fig. 5A). In contrast, the Pru*Δku80Δrop4/7*::*HXGPRT* mutant exhibited a 70% reduction in cyst burden at 5 weeks postinfection ($P = 0.0089$) (Fig. 5A). Significant reductions in cyst burdens compared to the parental Δ*ku80* Δ*hxgprt* strain were also observed in

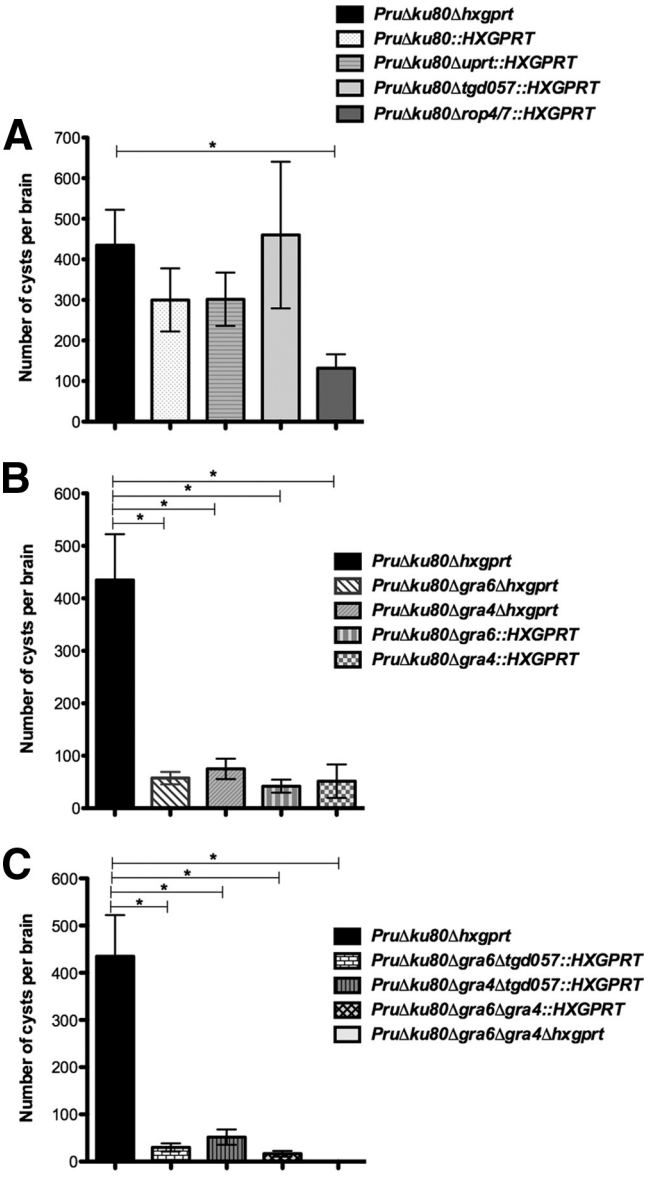

FIG. 5. Brain cyst burdens measured at 5 weeks postinfection. C57BL/6 mice were infected by intraperitoneal inoculation of 200 tachyzoites of mutant or parental strains. (A, B, and C) Brain cyst burdens in C57BL/6 mice. (A) Cyst burdens were measured at 5 weeks postinfection of C57BL/6 mice infected with the strain genotypes Δ*ku80*::*HXGPRT* (6 mice), Δ*ku80* Δ*hxgprt* (6 mice), Δ*ku80* Δ*uprt*::*HXGPRT* (6 mice), Δ*ku80* Δ*tgd057*::*HXGPRT* (6 mice), and Δ*ku80* Δ*rop4/7*::*HXGPRT* (6 mice). (B) Cyst burdens were measured at 5 weeks postinfection of C57BL/6 mice infected with the strain genotypes Δ*ku80* Δ*hxgprt* (6 mice), Δ*ku80* Δ*gra4*::*HXGPRT* (6 mice), Δ*ku80* Δ*gra6*::*HXGPRT* (6 mice), Δ*ku80* Δ*gra4* Δ*hxgprt* (4 mice), and Δ*ku80* Δ*gra6* Δ*hxgprt* (4 mice). (C) Cyst burdens were measured at 5 weeks postinfection of C57BL/6 mice infected with the strain genotypes Δ*ku80* Δ*hxgprt* (6 mice), Δ*ku80* Δ*gra4* Δ*tgd057*::*HXGPRT* (6 mice), Δ*ku80* Δ*gra6* Δ*tgd057*::*HXGPRT* (6 mice), Δ*ku80* Δ*gra6* Δ*gra4*::*HXGPRT* (6 mice), and Δ*ku80* Δ*gra6* Δ*gra4* Δ*hxgprt* (4 mice). Cyst data samples were subjected to a Student *t* test and are represented as means ± the SEM. Cyst burdens determined in mutant strains were compared to cyst burdens in the parental Δ*ku80* Δ*hxgprt* strain to establish significance ($P < 0.05$).

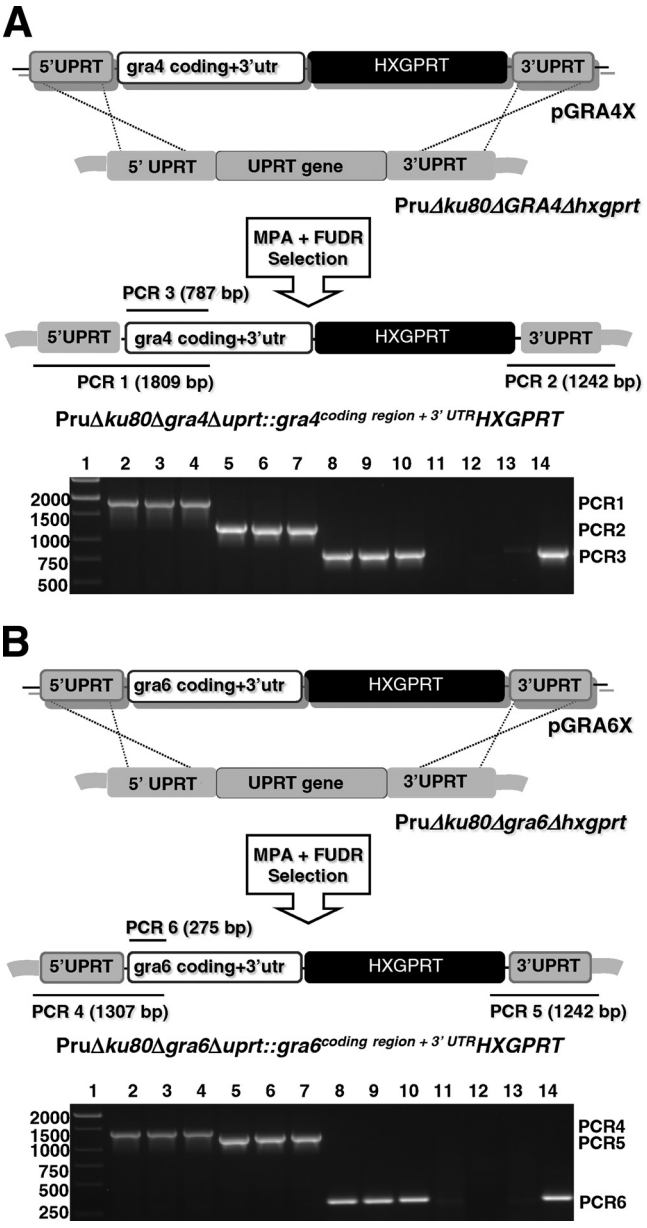

FIG. 6. Genetic strategy for complementation of the Δ*gra4* and Δ*gra6* deletion mutants. The coding region of the deleted GRA gene and the associated GRA 3′UTR was placed under regulatory control of the endogenous UPRT locus 5′UTR. (A) Plasmid pGRA4X was transfected into the Pru*Δku80Δgra4Δhxgprt* strain, and parasites were selected in MPA and then selected in FUDR to select for the Δ*uprt* phenotype. Clones isolated from this selection were examined using PCR 1, PCR 2, and PCR 3 to verify precise integration of the GRA4 coding region at the deleted *uprt* locus. PCR 1 measures correct 5′ integration, PCR 2 measures correct 3′ integration, and PCR 3 measures the presence of the GRA4 coding region. (Agarose gel panel) PCR 1, PCR 2, and PCR 3 products: DNA size ladder (lane 1), PCR 1 from 3 complemented clones (lanes 2 to 4), PCR 2 from 3 complemented clones (lanes 5 to 7), PCR 3 from 3 complemented clones (lanes 8 to 10), PCR 1 from parental Pru*Δku80Δgra4Δhxgprt* (lane 11), PCR 2 from parental Pru*Δku80Δgra4Δhxgprt* (lane 12), PCR 3 from parental Pru*Δku80Δgra4Δhxgprt* (lane 13), PCR 3 from Pru*Δku80Δhxgprt* (lane 14). (B) Plasmid pGRA6X was transfected into the Pru*Δku80Δgra6Δhxgprt* strain, and parasites were selected in MPA and then selected in FUDR to select for the Δ*uprt* phenotype. Clones isolated from this selection were examined using PCR 4, PCR 5, and PCR 6 to verify precise integration of the GRA6 coding region at the deleted *uprt* locus. PCR 4 measures correct 5′ integration, PCR 5 measures correct 3′ integration, and PCR 6 measures the presence of the GRA4 coding region. (Agarose gel panel) PCR 4, PCR 5, and PCR 6 products: DNA size ladder (lane 1), PCR 4 from three complemented clones (lanes 2 to 4), PCR 5 from three complemented clones (lanes 5 to 7), PCR 6 from three complemented clones (lanes 8 to 10), PCR 4 from parental Pru*Δku80Δgra6Δhxgprt* (lane 11), PCR 5 from parental Pru*Δku80Δgra6Δhxgprt* (lane 12), PCR 6 from parental Pru*Δku80Δgra6Δhxgprt* (lane 13), PCR 6 from Pru*Δku80Δhxgprt* (lane 14).

each of the Δ*gra4* and Δ*gra6* mutant strains examined at 5 weeks postinfection (Pru*Δku80Δgra4*::*HXGPRT* [$P = 0.0020$], Pru*Δku80Δgra6*::*HXGPRT* [$P = 0.0029$], Pru*Δku80Δgra4Δhxgprt* [$P = 0.011$], Pru*Δku80Δgra6Δhxgprt* [$P = 0.0087$], Pru*Δku80Δgra4Δtgd057*::*HXGPRT* [$P = 0.0015$], Pru*Δku80Δgra6Δtgd057*::*HXGPRT* [$P = 0.0010$], Pru*Δku80Δgra6Δgra4*::*HXGPRT* [$P = 0.0007$], Pru*Δku80Δgra6Δgra4Δhxgprt* [$P = 0.0040$]) (Fig. 5B and C).

Complementation of the Δ*gra4* and Δ*gra6* mutants. To more clearly establish that the defect in cyst burdens observed in the Δ*gra4* and Δ*gra6* mutant strains was due to the deletion of GRA protein function, we complemented the Δ*gra4* and Δ*gra6* mutants by reinserting a functional allele of the deleted *GRA* gene. Rather than simply recreating the parental strain with an intact GRA locus, we complemented the Δ*ku80* Δ*gra4* Δ*hxgprt* and the Δ*ku80* Δ*gra6* Δ*hxgprt* mutants by targeting the insertion of the GRA coding region and the *HXGPRT* marker into the *UPRT* locus, deleting the coding region of the *UPRT* gene (Fig. 6A and B). This strategy was based on our observation of normal cyst burdens in the Δ*ku80* Δ*uprt*::*hxgprt* mutant (Fig. 4A). In addition, by design we deleted the extremely strong *GRA4* and *GRA6* transcriptional promoters and their 5′ transcribed, untranslated region (5′ *GRA* UTRs), and via homologous recombination placed the GRA protein coding region(s) under the control of the endogenous *UPRT* locus 5′UTR which ranks at the ~ 78% for expression level percentile (microarray data [www.toxodb.org]) (Fig. 6). In contrast, the relative expression level percentile ranking is ~ 94.2% for the endogenous *GRA4* locus and ~99.2% for the endogenous *GRA6* locus. Parasites transfected with the pGRA4X and pGRA6X complementation cassettes were selected in MPA for 10 days then the population was selected in FUDR. Complemented clones were examined using a PCR strategy (Fig. 6) and correctly targeted clones with the genotypes Δ*ku80* Δ*gra4* Δ*uprt*::*gra4*$^{\text{coding region + 3′UTR}}$ *HXGPRT* and Δ*ku80* Δ*gra6* Δ*uprt*::*gra6*$^{\text{coding region + 3′UTR}}$ *HXGPRT* were validated (Fig. 6).

Two independent cloned isolates of each complemented strain were examined for cyst burden in C57BL/6 mice at 3 weeks postinfection. GRA4 complemented clones exhibited a 402 to 426% increase in cyst burdens compared to the Δ*gra4* mutant strain also lacking *HXGPRT* (*GRA4*, $P = 0.0010$ and $P = 0.024$) (Fig. 7). GRA6 complemented clones exhibited a 291 to 352% increase in cyst burdens compared to the Δ*gra6* mutant strain also lacking *HXGPRT* (*GRA6*, $P = 0.032$ and $P = 0.031$) (Fig. 7).

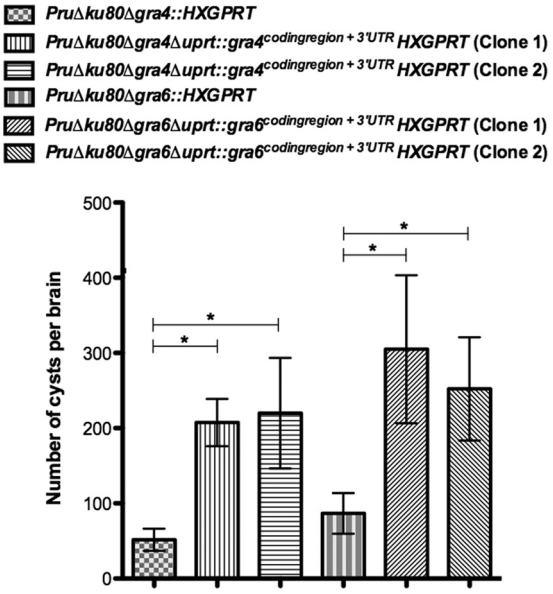

FIG. 7. Cyst burdens are significantly increased in the GRA-complemented strains. C57BL/6 mice were infected by intraperitoneal inoculation of 200 tachyzoites of mutant parental or complemented strains. Cyst burdens were measured at 3 weeks postinfection of C57BL/6 mice infected with the strains Pru*Δku80Δgra4*::*HXGPRT* (6 mice), Pru*Δku80Δgra4Δuprt*::*gra4*$^{\text{coding region + 3'UTR}}$*HXGPRT* (clone 1, 4 mice, and clone 2, 4 mice), Pru*Δku80Δgra6*::*HXGPRT* (6 mice), Pru*Δku80Δgra6Δuprt*::*gra6*$^{\text{coding region + 3'UTR}}$*HXGPRT* (clone 1, 4 mice, and clone 2, 4 mice). Cyst data samples were subjected to a Student *t* test and are represented as means ± the SEM. Cyst burdens determined in complemented strains were compared to cyst burdens in the parental Δ*gra* strain to establish significance ($P < 0.05$).

DISCUSSION

Type II isolates of *T. gondii* represent a prevalent strain type infecting humans and causing life-long infections characterized by the presence of the bradyzoite stage encysted tissue cyst. Previously, targeted genetic dissection of type II *T. gondii* strains was limited by inefficient homologous recombination pathways relative to highly efficient pathways for random integration of targeting episomes. By eliminating the dominant pathway of nonhomologous recombination via knockout and functional disruption of the *KU80* gene (26), we now report a new genetic model that enables efficient gene replacements and the reliable development of targeted gene deletions in type II *T. gondii*.

The Pru*Δku80Δhxgprt* strain exhibited efficient gene targeting at the *UPRT* locus, at the *OPRT* locus, and at all other targeted loci. Efficient gene targeting was demonstrated to be dependent on perfect DNA sequence homology. We successfully targeted seven genetic loci for deletion (*UPRT*, *UP*, *OPRT*, *GRA4*, *GRA6*, *ROP4*/*7*, and *tgd057*), we retargeted the deletion of *HXGPRT* inserted at three disrupted loci (*OPRT*, *GRA4*, *GRA6*), we constructed three mutant strains with two targeted gene deletions (Δ*gra4* Δ*gra6*, Δ*gra4* Δ*tgd057*, and Δ*gra6* Δ*tgd057*), and we functionally complemented the *GRA4* and *GRA6* knockouts. These results show that the type II *Δku80 Δhxgprt* genetic background is amenable for rapid and reliable development of targeted gene deletions, and other more complex genetic manipulations involving sequential targeting, removal of *HXGPRT* at the deleted locus, and retargeting using *HXGPRT*. The ability of the Pru*Δku80Δhxgprt* strain to develop cyst burdens and latent infection was maintained after long-term *in vitro* culture or multiple genetic manipulations. In addition, the Pru*Δku80Δhxgprt* strain retained a normal intracellular replication rate compared to the parental Pru strain, and this strain also retains normal acute virulence in mice (data not shown). The type I *KU80* knockout strain RH*Δku80Δhxgprt* retains a normal intracellular replication rate, acute virulence in mice (26), and this strain also exhibits an identical profile of gene expression during the cell cycle as parental RH (3). Collectively, these results support the Pru*Δku80Δhxgprt* genetic background as an improved genetic model for dissecting type II *T. gondii* biology.

Type II mutants deleted in pyrimidine salvage activities for UPRT and UP were not defective in cyst development, demonstrating that pyrimidine salvage through the UPRT or UP enzyme activities is not required for cyst development or the establishment of latent infection. These results suggest that *de novo* pyrimidine synthesis is functional and essential during bradyzoite stage conversion, cyst development, and latent infection.

We examined the hypothesis that host $CD8^+$ T cell responses directed against specific parasite antigens containing $CD8^+$ T cell epitopes (GRA4, GRA6, ROP7, and tgd057) (5, 27, 42, 68) may influence cyst development. Our analysis was hindered by the low cyst burdens (<60 cysts per brain) that we observed in the H-$2L^d$-restricted BALB/c background. The H-$2L^d$-restricted BALB/c background is genetically resistant to infection and establishes a latent infection with reduced cyst burdens compared to genetically susceptible murine backgrounds such as C57BL/6, which exhibit higher cyst burdens, reactivation, and chronic infection (30, 45, 56). Recent observations suggest that infection of genetically susceptible C57BL/6 mice with the Pru strain produces the highest brain tissue cyst burden at 3 weeks postinfection (56), then cysts rupture (reactivate) and are lost at a higher rate than any potential rate of cyst reformation during chronic infection. Immune control of type II *T. gondii* infection has been proposed to be dependent on type II strain-specific H-$2L^d$-restricted cytotoxic T cells (35). This hypothesis is supported by the identification of the immunodominant and protective decapeptide HF10 epitope within the type II GRA6 protein that is presented in the context of the H-$2L^d$ major histocompatibility complex class I molecule (5).

The previously identified GRA4, GRA6, and ROP7 $CD8^+$ T cell epitopes are H-$2L^d$-restricted (5, 27), whereas the tdg057 $CD8^+$ T cell epitope is H-$2K^b$ restricted. Consequently, in C57BL/6 mice a $CD8^+$ T cell response is mounted against the known tdg057 epitope (68), but not against the known GRA4, GRA6, or ROP7 epitopes. At 3 weeks postinfection of C57BL/6 mice, we observed no significant differences in cyst burdens in either the Δ*rop4*/*7* or the Δ*tgd057* mutants compared to the Δ*ku80* Δ*hxgprt* parent. The absence of $CD8^+$ T cell response to the tgd057 epitope, as well as the loss of tgd057 protein function in the Δ*tgd057* mutant, did not significantly affect cyst burdens. Similarly, the absence of $CD8^+$ T cell response to ROP7 in both the parental strain and the Δ*rop4*/*7* mutant, along with the loss of ROP4/7 protein functions, did not significantly affect cyst burdens at 3 weeks postinfection. In

contrast, while the $CD8^+$ T cell response to the GRA4 and GRA6 epitopes is absent in the parental strain in the C57BL/6 murine background, the deletion of the *GRA4* (Δ*gra4*) and *GRA6* (Δ*gra6*) genes markedly reduced cyst burdens independently of any potential $CD8^+$ T cell response to the known epitopes within these GRA proteins. However, we cannot conclusively rule out the possibility that the *GRA4* and/or *GRA6* genes encode as-yet-uncharacterized H-$2K^b$-restricted epitopes. We also observed a significant defect in cyst burdens in the Δ*gra4* and Δ*gra6* mutants in the CBA murine background (H-$2K^k$-restricted). These results suggest that the GRA4 and GRA6 proteins directly mediate functions necessary for the development of normal cyst burdens, rather than cyst development being strictly dependent on the host response to these proteins.

Previous studies have also reported defects in cyst development following gene disruption in type II strains. Disruption of the *SRS9* gene or the *SAG2CDXY* gene locus revealed a phenotype of normal cyst burdens at 4 weeks postinfection, and then reduced cyst burdens were observed later during latent infection (41, 55). Disruption of a pseudouridine synthase homologue (*PUS1*) revealed a phenotype of slightly smaller cyst size and slightly increased cyst burdens (1). Targeted disruption of the heat shock protein *BAG1* gene (6, 69) resulted in a minor defect in cyst development. A significant defect in cyst burden was observed at 5 weeks postinfection in the Δ*rop4*/*7* mutant. Interestingly, the Δ*rop4*/*7* mutant and the Δ*tgd057* mutant exhibited an increase in their *in vitro* growth rate. The recently reported type II GRA15 knockout was also reported to exhibit an increased growth rate *in vitro* (54).

Cross-linking studies suggest that a multimeric protein complex of GRA2, GRA4, and GRA6 exists within the nanotubular network of membranes within the parasitophorous vacuole space (43). However, a recent study of protein interactions using a more comprehensive panel of HA-FLAG-tagged GRA proteins did not reveal a direct interaction of GRA2, GRA4, and GRA6 in the membrane fraction (8). Disruption of *GRA6* in type I tachyzoites revealed an altered intravacuolar network of membranes characterized by small vesicles instead of elongated nanotubules (47). The N terminus of GRA6 was also recently shown to be a critical domain in interacting with negatively charged lipids and is necessary for association of the protein with the vacuolar membranous network of nanotubules (28).

Type II mutants with *GRA4* or *GRA6* deleted exhibited drastically reduced cyst burdens during *T. gondii* infection. The defect in cyst development in these strains was independent of the presence or absence of *HXGPRT*. Thus, these GRA proteins appear to be involved in some aspect of cyst development that significantly reduces the likelihood of cyst formation rather than completely abrogating the parasites biological ability to convert to the bradyzoite stage and create a tissue cyst. Complementation of the Δ*gra4* and Δ*gra6* mutants using a functional allele of the corresponding GRA protein significantly restored cyst burdens. However, cyst burdens were not completely restored to the expected levels when *GRA4* and *GRA6* expression was placed under regulatory control of the *UPRT* locus. The relative strengths of the *GRA4* and *GRA6* promoters (*GRA4*, ~94.2%; *GRA6*, ~99.2% [www.toxodb.org]) are significantly higher than that of the *UPRT* locus (~78%) used in the complementation study. These observations suggest that an extremely high level of expression of GRA4 and GRA6 may be necessary for the development of normal cyst burdens.

A more severe defect in cyst burden in the Δ*ku80*Δ*gra6*Δ*gra4*::*HXGPRT* and the Δ*ku80* Δ*gra6* Δ*gra4* Δ*hxgprt* mutants compared to mutants with single deletions of *GRA4* or *GRA6* suggests that GRA4 and GRA6 most likely play independent functional roles required for cyst development during infection. Ultrastructural localization is also consistent with the likelihood of independent roles for GRA4 and GRA6 in cyst development since, while GRA4 is abundant in the tachyzoite stage, PV it is not detectable in the bradyzoite stage cyst wall, whereas GRA6 is easily detected in both stages (21). Since the cyst wall structure is thought to arise directly from modifications to the PVM during tachyzoite to bradyzoite conversion (59, 67), the function of GRA4 in cyst development is likely to be exerted prior to or during formation of the cyst wall.

Our study did not specifically address the mechanisms by which GRA4 or GRA6 influence cyst development. With the exception of uracil auxotrophy of the Δ*oprt* mutants, no significant decreases were observed in the *in vitro* replication rate of any of the mutants isolated in the present study. The defect in cyst burden in the Δ*gra4* and Δ*gra6* mutants may be due to a more successful innate or adaptive host response that suppresses parasite burden or dissemination necessary for development of brain tissue cysts. Alternatively, GRA4 and GRA6 may play a direct role in parasite biology associated with the probability of successful tachyzoite to bradyzoite conversion or cyst development. Additional studies are therefore necessary to assess acute virulence, parasite tissue burdens, dissemination patterns, and host response during infection to further gauge potential mechanisms underlying the defect in cyst development in the Δ*gra4* and Δ*gra6* mutants.

The GRA protein family is extremely interesting because they are a remarkable family of highly expressed and compartmentalized proteins restricted thus far to the cyst-forming parasites *Toxoplasma* and *Neospora* (49). No identifiable ortholog can be discerned even in closely related Conoidasida such as *Cryptosporidium* or *Eimeria* or Aconoidasida such as *Plasmodium*, which do not form tissue cysts (10). Our results suggest that in addition to GRA4 and GRA6 other members of the prominent GRA protein family may also play critical roles in biology underlying successful cyst development and latent infection.

The type II Δ*ku80* Δ*hxgprt* strain developed in the present study provides a reliable genetic model for targeted genetic dissection of parasite biology occurring during *T. gondii* infection. The ability to now control both parasite genes and host cell genes can reveal the complex interplay of parasite biology and host response during *T. gondii* infection. These genetic approaches will accelerate the development of improved strategies for vaccines, immunological interventions, and other therapeutics. Targeted genetic approaches using a type II Δ*ku80* Δ*hxgprt* genetic background has the immediate potential to functionally reveal parasite genes playing critical biological roles that, when intercepted during *in vivo* infection, block parasite development, pathogenesis, or transmission.

ACKNOWLEDGMENTS

We are grateful to numerous *Toxoplasma* research laboratories that provided helpful advice and suggestions during the course of this study. This project was made possible by the work of the developers of the *Toxoplasma gondii* Genome Resource (at www.ToxoDB.org), and their work is gratefully acknowledged. ToxoDB, PlasmoDB, and EuPathDB are part of the National Institutes of Health/National Institute of Allergy and Infectious Disease (NIH/NIAID)-funded Bioinformatics Resource Center. Type II strains were kindly provided by John Boothroyd (Stanford University), Jeroen Saeij (Massachusetts Institute of Technology), and Elmer Pfefferkorn (Dartmouth College). This study was supported by the use of facilities that were provided by the Imaging Shared Resource of the Dartmouth-Hitchcock Norris Cotton Cancer Center.

L.M.R. was a predoctoral trainee on NIH training grant T32AI007519 on Host-Microbe Interactions. This study was supported by the NIH (grant AI039454 to L.M.W. and grants AI41930, AI073142, AI075931, and AI091461 to D.J.B.).

REFERENCES

1. **Anderson, M. Z., J. Brewer, U. Singh, and J. C. Boothroyd.** 2009. A pseudouridine synthase homologue is critical to cellular differentiation in *Toxoplasma gondii*. Eukaryot. Cell **8:**398–409.
2. **Beck, J. R., et al.** 2010. A novel family of *Toxoplasma* IMC proteins displays a hierarchical organization and functions in coordinating parasite division. PLoS Pathog. **6:**e1001094.
3. **Behnke, M. S., et al.** 2010. Coordinated progression through two subtranscriptomes underlies the tachyzoite cycle of *Toxoplasma gondii*. PLoS One **5:**e12354.
4. **Bierly, A. L., W. J. Shufesky, W. Sukhumavasi, A. E. Morelli, and E. Y. Denkers.** 2008. Dendritic cells expressing plasmacytoid marker PDCA-1 are Trojan horses during *Toxoplasma gondii* infection. J. Immunol. **181:**8485–8491.
5. **Blanchard, N., et al.** 2008. Immunodominant, protective response to the parasite *Toxoplasma gondii* requires antigen processing in the endoplasmic reticulum. Nat. Immunol. **9:**937–944.
6. **Bohne, W., et al.** 1998. Targeted disruption of the bradyzoite-specific gene BAG1 does not prevent tissue cyst formation in *Toxoplasma gondii*. Mol. Biochem. Parasitol. **92:**291–301.
7. **Boothroyd, J. C., and J. F. Dubremetz.** 2008. Kiss and spit: the dual roles of *Toxoplasma* rhoptries. Nat. Rev. Microbiol. **6:**79–88.
8. **Braun, L., et al.** 2008. Purification of *Toxoplasma* dense granule proteins reveals that they are in complexes throughout the secretory pathway. Mol. Biochem. Parasitol. **157:**13–21.
9. **Carruthers, V. B., and L. D. Sibley.** 1997. Sequential protein secretion from three distinct organelles of *Toxoplasma gondii* accompanies invasion of human fibroblasts. Eur. J. Cell Biol. **73:**114–123.
10. **Cesbron-Delauw, M. F., C. Gendrin, L. Travier, P. Ruffiot, and C. Mercier.** 2008. Apicomplexa in mammalian cells: trafficking to the parasitophorous vacuole. Traffic **9:**657–664.
11. **Chtanova, T., et al.** 2008. Dynamics of neutrophil migration in lymph nodes during infection. Immunity **29:**487–496.
12. **Contini, C.** 2008. Clinical and diagnostic management of toxoplasmosis in the immunocompromised patient. Parasitologia **50:**45–50.
13. **Craver, M. P., and L. J. Knoll.** 2007. Increased efficiency of homologous recombination in *Toxoplasma gondii* dense granule protein 3 demonstrates that GRA3 is not necessary in cell culture but does contribute to virulence. Mol. Biochem. Parasitol. **153:**149–157.
14. **Denkers, E. Y., and B. A. Butcher.** 2005. Sabotage and exploitation in macrophages parasitized by intracellular protozoans. Trends Parasitol. **21:**35–41.
15. **Dixon, S. E., M. M. Bhatti, V. N. Uversky, A. K. Dunker, and W. J. Sullivan, Jr.** 2011. Regions of intrinsic disorder help identify a novel nuclear localization signal in *Toxoplasma gondii* histone acetyltransferase TgGCN5-B. Mol. Biochem. Parasitol. **175:**192–195.
16. **Donald, R. G., D. Carter, B. Ullman, and D. S. Roos.** 1996. Insertional tagging, cloning, and expression of the *Toxoplasma gondii* hypoxanthine-xanthine-guanine phosphoribosyltransferase gene. Use as a selectable marker for stable transformation. J. Biol. Chem. **271:**14010–14019.
17. **Donald, R. G., and D. S. Roos.** 1995. Insertional mutagenesis and marker rescue in a protozoan parasite: cloning of the uracil phosphoribosyltransferase locus from *Toxoplasma gondii*. Proc. Natl. Acad. Sci. U. S. A. **92:**5749–5753.
18. **Donald, R. G., and D. S. Roos.** 1993. Stable molecular transformation of *Toxoplasma gondii*: a selectable dihydrofolate reductase-thymidylate synthase marker based on drug-resistance mutations in malaria. Proc. Natl. Acad. Sci. U. S. A. **90:**11703–11707.
19. **Dubey, J. P.** 2007. The history and life cycle of *Toxoplasma gondii*, p. 1–18. *In* L. M. Weiss et al. (ed.), *Toxoplasma gondii*: the model apicomplexan parasite: perspectives and methods. Elsevier, London, United Kingdom.
20. **Fentress, S. J., et al.** 2010. Phosphorylation of immunity-related GTPases by a *Toxoplasma gondii*-secreted kinase promotes macrophage survival and virulence. Cell Host Microbe **8:**484–495.
21. **Ferguson, D. J.** 2004. Use of molecular and ultrastructural markers to evaluate stage conversion of *Toxoplasma gondii* in both the intermediate and definitive host. Int. J. Parasitol. **34:**347–360.
22. **Fox, B. A., A. A. Belperron, and D. J. Bzik.** 1999. Stable transformation of *Toxoplasma gondii* based on a pyrimethamine-resistant trifunctional dihydrofolate reductase-cytosine deaminase-thymidylate synthase gene that confers sensitivity to 5-fluorocytosine. Mol. Biochem. Parasitol. **98:**93–103.
23. **Fox, B. A., and D. J. Bzik.** 2010. Avirulent uracil auxotrophs based on disruption of orotidine-5′-monophosphate decarboxylase elicit protective immunity to *Toxoplasma gondii*. Infect. Immun. **78:**3744–3752.
24. **Fox, B. A., and D. J. Bzik.** 2002. De novo pyrimidine biosynthesis is required for virulence of *Toxoplasma gondii*. Nature **415:**926–929.
25. **Fox, B. A., J. G. Ristuccia, and D. J. Bzik.** 2009. Genetic identification of essential indels and domains in carbamoyl phosphate synthetase II of *Toxoplasma gondii*. Int. J. Parasitol. **39:**533–539.
26. **Fox, B. A., J. G. Ristuccia, J. P. Gigley, and D. J. Bzik.** 2009. Efficient gene replacements in *Toxoplasma gondii* strains deficient for nonhomologous end joining. Eukaryot. Cell **8:**520–529.
27. **Frickel, E. M., et al.** 2008. Parasite stage-specific recognition of endogenous *Toxoplasma gondii*-derived $CD8^+$ T cell epitopes. J. Infect. Dis. **198:**1625–1633.
28. **Gendrin, C., A. Bittame, C. Mercier, and M. F. Cesbron-Delauw.** 2010. Post-translational membrane sorting of the *Toxoplasma gondii* GRA6 protein into the parasite-containing vacuole is driven by its N-terminal domain. Int. J. Parasitol. **40:**1325–1334.
29. **Gigley, J. P., B. A. Fox, and D. J. Bzik.** 2009. Cell-mediated immunity to *Toxoplasma gondii* develops primarily by local Th1 host immune responses in the absence of parasite replication. J. Immunol. **182:**1069–1078.
30. **Gigley, J. P., B. A. Fox, and D. J. Bzik.** 2009. Long-term immunity to lethal acute or chronic type II *Toxoplasma gondii* infection is effectively induced in genetically susceptible C57BL/6 mice by immunization with an attenuated type I vaccine strain. Infect. Immun. **77:**5380–5388.
31. **Gubbels, M. J., B. Striepen, N. Shastri, M. Turkoz, and E. A. Robey.** 2005. Class I major histocompatibility complex presentation of antigens that escape from the parasitophorous vacuole of *Toxoplasma gondii*. Infect. Immun. **73:**703–711.
32. **Holpert, M., U. Gross, and W. Bohne.** 2006. Disruption of the bradyzoite-specific P-type (H^+)-ATPase PMA1 in *Toxoplasma gondii* leads to decreased bradyzoite differentiation after stress stimuli but does not interfere with mature tissue cyst formation. Mol. Biochem. Parasitol. **146:**129–133.
33. **Howe, D. K., S. Honore, F. Derouin, and L. D. Sibley.** 1997. Determination of genotypes of *Toxoplasma gondii* strains isolated from patients with toxoplasmosis. J. Clin. Microbiol. **35:**1411–1414.
34. **Huynh, M. H., and V. B. Carruthers.** 2009. Tagging of endogenous genes in a *Toxoplasma gondii* strain lacking Ku80. Eukaryot. Cell **8:**530–539.
35. **Johnson, J. J., et al.** 2002. In vitro correlates of Ld-restricted resistance to toxoplasmic encephalitis and their critical dependence on parasite strain. J. Immunol. **169:**966–973.
36. **Jones, J. L., and G. N. Holland.** 2010. Annu. burden of ocular toxoplasmosis in the US. Am. J. Trop. Med. Hyg. **82:**464–465.
37. **Joyce, B. R., S. F. Queener, R. C. Wek, and W. J. Sullivan, Jr.** 2010. Phosphorylation of eukaryotic initiation factor-2α promotes the extracellular survival of obligate intracellular parasite *Toxoplasma gondii*. Proc. Natl. Acad. Sci. U. S. A. **107:**17200–17205.
38. **Karasov, A. O., J. C. Boothroyd, and G. Arrizabalaga.** 2005. Identification and disruption of a rhoptry-localized homologue of sodium hydrogen exchangers in *Toxoplasma gondii*. Int. J. Parasitol. **35:**285–291.
39. **Kim, K., D. Soldati, and J. C. Boothroyd.** 1993. Gene replacement in *Toxoplasma gondii* with chloramphenicol acetyltransferase as selectable marker. Science **262:**911–914.
40. **Kim, K., and L. M. Weiss.** 2008. *Toxoplasma*: the next 100 years. Microbes Infect. **10:**978–984.
41. **Kim, S. K., A. Karasov, and J. C. Boothroyd.** 2007. Bradyzoite-specific surface antigen SRS9 plays a role in maintaining *Toxoplasma gondii* persistence in the brain and in host control of parasite replication in the intestine. Infect. Immun. **75:**1626–1634.
42. **Kirak, O., et al.** 2010. Transnuclear mice with predefined T cell receptor specificities against *Toxoplasma gondii* obtained via SCNT. Science **328:**243–248.
43. **Labruyere, E., M. Lingnau, C. Mercier, and L. D. Sibley.** 1999. Differential membrane targeting of the secretory proteins GRA4 and GRA6 within the parasitophorous vacuole formed by *Toxoplasma gondii*. Mol. Biochem. Parasitol. **102:**311–324.
44. **Larson, E. T., et al.** 2009. *Toxoplasma gondii* cathepsin L is the primary target of the invasion-inhibitory compound morpholinurea-leucyl-homophenyl-vinyl sulfone phenyl. J. Biol. Chem. **284:**26839–26850.
45. **McLeod, R., E. Skamene, C. R. Brown, P. B. Eisenhauer, and D. G. Mack.** 1989. Genetic regulation of early survival and cyst number after peroral

Toxoplasma gondii infection of A×B/B×A recombinant inbred and B10 congenic mice. J. Immunol. **143:**3031–3034.
46. **Mercier, C., M. F. Cesbron-Delauw, and D. J. P. Ferguson.** 2007. Dense granules of the infectious stages of *Toxoplasma gondii*: their central role in the host/parasite relationship, p. 475–492. *In* D. S. Ajioka et al. (ed.), *Toxoplasma*: molecular and cellular biology. Horizon Bioscience, Norfolk, United Kingdom.
47. **Mercier, C., et al.** 2002. Biogenesis of nanotubular network in *Toxoplasma* parasitophorous vacuole induced by parasite proteins. Mol. Biol. Cell **13:** 2397–2409.
48. **Mercier, C., D. K. Howe, D. Mordue, M. Lingnau, and L. D. Sibley.** 1998. Targeted disruption of the *GRA2* locus in *Toxoplasma gondii* decreases acute virulence in mice. Infect. Immun. **66:**4176–4182.
49. **Mercier, C., L. Travier, A. Bittame, C. Gendrin, and M. F. Cesbraun-Delauw.** 2010. The dense granule proteins of *Toxoplasma gondii*, p. 1–31. *In* O. De Bruyn and S. Peeters (ed.), Parasitology research trends. Nova Science Publishers, Hauppage, NY.
50. **Montoya, J. G., and J. S. Remington.** 2008. Management of *Toxoplasma gondii* infection during pregnancy. Clin. Infect. Dis. **47:**554–566.
51. **Odaert, H., M. Soete, B. Fortier, D. Camus, and J. F. Dubremetz.** 1996. Stage conversion of *Toxoplasma gondii* in mouse brain during infection and immunodepression. Parasitol. Res. **82:**28–31.
52. **Robben, P. M., and L. D. Sibley.** 2004. Food- and waterborne pathogens: you are (infected by) what you eat! Microbes Infect. **6:**406–413.
53. **Roos, D. S.** 2005. Genetics: themes and variations in apicomplexan parasite biology. Science **309:**72–73.
54. **Rosowski, E. E., et al.** 2011. Strain-specific activation of the NF-κB pathway by GRA15, a novel *Toxoplasma gondii* dense granule protein. J. Exp. Med. **208:**195–212.
55. **Saeij, J. P., G. Arrizabalaga, and J. C. Boothroyd.** 2008. A cluster of four surface antigen genes specifically expressed in bradyzoites, SAG2CDXY, plays an important role in *Toxoplasma gondii* persistence. Infect. Immun. **76:**2402–2410.
56. **Schaeffer, M., et al.** 2009. Dynamic imaging of T cell-parasite interactions in the brains of mice chronically infected with *Toxoplasma gondii*. J. Immunol. **182:**6379–6393.
57. **Schwarz, J. A., A. E. Fouts, C. A. Cummings, D. J. Ferguson, and J. C. Boothroyd.** 2005. A novel rhoptry protein in *Toxoplasma gondii* bradyzoites and merozoites. Mol. Biochem. Parasitol. **144:**159–166.
58. **Sibley, L. D., and J. W. Ajioka.** 2008. Population structure of *Toxoplasma gondii*: clonal expansion driven by infrequent recombination and selective sweeps. Annu. Rev. Microbiol. **62:**329–351.
59. **Sinai, A. P.** 2008. Biogenesis of and activities at the *Toxoplasma gondii* parasitophorous vacuole membrane. Subcell. Biochem. **47:**155–164.
60. **Singh, U., J. L. Brewer, and J. C. Boothroyd.** 2002. Genetic analysis of tachyzoite to bradyzoite differentiation mutants in *Toxoplasma gondii* reveals a hierarchy of gene induction. Mol. Microbiol. **44:**721–733.
61. **Soldati, D., and J. C. Boothroyd.** 1993. Transient transfection and expression in the obligate intracellular parasite *Toxoplasma gondii*. Science **260:**349–352.
62. **Su, C., et al.** 2003. Recent expansion of *Toxoplasma* through enhanced oral transmission. Science **299:**414–416.
63. **Suzuki, Y., and J. S. Remington.** 1988. Dual regulation of resistance against *Toxoplasma gondii* infection by Lyt-2^+ and Lyt-1^+, L3T4^+ T cells in mice. J. Immunol. **140:**3943–3946.
64. **Torpier, G., et al.** 1993. *Toxoplasma gondii*: differential location of antigens secreted from encysted bradyzoites. Exp. Parasitol. **77:**13–22.
65. **Vanchinathan, P., J. L. Brewer, O. S. Harb, J. C. Boothroyd, and U. Singh.** 2005. Disruption of a locus encoding a nucleolar zinc finger protein decreases tachyzoite-to-bradyzoite differentiation in *Toxoplasma gondii*. Infect. Immun. **73:**6680–6688.
66. **Wallace, G. R., and M. R. Stanford.** 2008. Immunity and *Toxoplasma* retinochoroiditis. Clin. Exp. Immunol. **153:**309–315.
67. **Weiss, L. M., and K. Kim.** 2000. The development and biology of bradyzoites of *Toxoplasma gondii*. Front. Biosci. **5:**D391–D405.
68. **Wilson, D. C., et al.** 2010. Differential regulation of effector- and central-memory responses to *Toxoplasma gondii* infection by IL-12 revealed by tracking of Tgd057-specific $CD8^+$ T cells. PLoS Pathog. **6:**e1000815.
69. **Zhang, Y. W., et al.** 1999. Disruption of the *Toxoplasma gondii* bradyzoite-specific gene *BAG1* decreases in vivo cyst formation. Mol. Microbiol. **31:** 691–701.